Quantum gases in trimerized kagomé lattices

B. Damski,[1,2] H. Fehrmann,[1] H.-U. Everts,[1] M. Baranov,[3,4] L. Santos,[5] and M. Lewenstein[1,6,*]
[1]*Institut für Theoretische Physik, Universität Hannover, D-30167 Hannover, Germany*
[2]*Theory Division, Los Alamos National Laboratory, MS-B213, Los Alamos, New Mexico 87545, USA*
[3]*Van der Waals–Zeeman Instituut, Universiteit van Amsterdam, 1018 XE Amsterdam, The Netherlands*
[4]*Kurchatov Institute, Kurchatov square 1, 123182 Moscow, Russia*
[5]*Institut für Theoretische Physik III, Universität Stuttgart, D-70550 Stuttgart, Germany*
[6]*ICFO–Institut de Ciències Fotòniques, Jordi Girona 29, Edifici Nexus II, E-08034 Barcelona, Spain*
(Received 6 July 2005; published 10 November 2005)

We study low-temperature properties of atomic gases in trimerized optical kagomé lattices. The laser arrangements that can be used to create these lattices are briefly described. We also present explicit results for the coupling constants of the generalized Hubbard models that can be realized in such lattices. In the case of a single-component Bose gas the existence of a Mott insulator phase with fractional numbers of particles per trimer is verified in a mean-field approach. The main emphasis of the paper is on an atomic spinless interacting Fermi gas in the trimerized kagomé lattice with two fermions per site. This system is shown to be described by a quantum spin-1/2 model on the triangular lattice with couplings that depend on the bond directions. We investigate this model by means of exact diagonalization. Our key finding is that the system exhibits nonstandard properties of a quantum spin-liquid crystal: it combines planar antiferromagnetic order in the ground state with an exceptionally large number of low-energy excitations. The possibilities of experimental verification of our theoretical results are critically discussed.

DOI: 10.1103/PhysRevA.72.053612 PACS number(s): 03.75.Ss, 05.30.Jp, 05.30.Fk

I. INTRODUCTION

The experimental realization of the Bose-Einstein condensation (BEC) [1] linked the physics of cold atoms with that of weakly interacting many-body systems, traditionally studied by condensed-matter physics. More recently, the seminal theory paper by Jaksch *et al.* [2], followed by equally seminal experiments by Greiner *et al.* [3], on the Mott insulator (MI) to superfluid (SF) transition have paved the way toward the analysis of strongly correlated systems within the physics of cold atoms. In this sense, the physics of cold atoms is nowadays merging with condensed-matter physics, solid-state physics, and quantum information at the same common frontiers and open challenging problems, such as, for instance, the BEC-BCS crossover (see for instance [4]), fractional quantum Hall effect (cf. [5]), the physics of one-dimensional (1D) systems [6], etc. Quantum information has given new impulses toward the understanding of quantum phase transitions [7], and to understand better the known (and develop new) numerical methods of treating many-body systems [8].

A. Atomic lattice gases

One of most fascinating playgrounds of cold-atom physics is provided by ultracold lattice gases, i.e., cold atoms trapped in optical lattices produced by standing laser waves where, in the case of red- (blue-)detuned laser light, the potential minima coincide with the intensity maxima (minima) [9]. This technique has been of enormous interest during resent years. The setup can be chosen to be one, two, or three dimensional, where the lattice forms range from simple periodic (such as a square in 2D, or a cubic lattice in 3D, respectively) to more exotic lattices, such as hexagonal [10] or kagomé [11] lattices, created with the use of superlattice techniques [12]. In experiments, optical lattices offer an unprecedentedly wide range of tunable parameters, which can be changed during the evolution *in situ* and "*in vivo*," i.e., in real time. These possibilities, on one hand, link strongly the physics of ultracold atoms in optical lattices to various areas of condensed-matter physics, and on the other, they open completely new ways to study quantum many-body systems, to perform in various ways quantum-information processing (cf. [13,14]), and even to realize special purpose quantum computers, so-called quantum simulators [15].

The physics of ultracold atomic gases in optical lattices is in general described by various versions of the Hubbard model, which is probably the most important and structurally simple model of condensed-matter physics, capable nevertheless of describing an enormous variety of physical phenomena and effects [16,17]. Atomic ultracold gases may serve as a "Hubbard model toolkit" [18], and several models have been discussed in more detail in this context: the most simple Bose-Hubbard model [2] (for the seminal condensed-matter treatment see [19]), the Fermi-Fermi model (which should eventually allow for quantum simulations of high-T_c superconductivity [20]) the Fermi-Bose model (which leads to creation of composite fermions via fermion-boson or fermion–bosonic hole pairing, cf. [21,22]), or Bose-Bose, or more generally multicomponent systems. Quenched disorder may be introduced in a controlled way to such systems [23,24], which opens the possibility of studying the physics of disordered systems in this framework.

*Also at Institució Catalana de Recerca i Estudis Avançats.

In a certain limit Hubbard models reduce to spin models and this possibility has been also intensively investigated recently for both atomic gases [10,25,26], and ion chains [27]. Spin models enjoy particular interest because of their simplicity and thus possible applicability in quantum-information processing (cf. [26,28]). In this paper we will discuss yet another possibility, i.e., the possibility of studying frustrated quantum antiferromagnets (AFM's).

B. Quantum antiferromagnets

Quantum antiferromagnets, and in particular frustrated AFM's are in the center of interest of modern condensed-matter physics (for a recent review, see [29]). One of the reasons for this interest is that frustrated AFM's are believed to explain certain aspects of high-T_c superconductivity [16]. In this context frustrated spin-1/2 models have attracted particular attention. At the same time almost all of these models are notoriously difficult to handle analytically and numerically. The only exceptions are those models that exhibit long-range Néel-type order, since there is a powerful method by which long-range order can be identified numerically (see, e.g., [30]), and if it exists, the semiclassical (spin-wave) approximation yields satisfactory results. In 2D only very few exactly solvable spin-1/2 models are known [29]. In 1D exact results can be obtained by the Bethe-ansatz technique in a number of cases [31]. Moreover, nonperturbative bosonization techniques and powerful numerical methods such as the density matrix renormalization group (DMRG) method can be applied. However, DMRG techniques become very difficult to handle in the case of disordered systems [32]. In 2D, in the absence of long-range order, apart from renormalization group approaches, numerical methods offer the only possibility to investigate frustrated spin systems. However, quantum Monte Carlo (QMC) simulations of Heisenberg AFM's on frustrated lattices, such as the triangular and the kagomé lattice, suffer from the "negative sign" problem. For instance, attempts to obtain useful results for the Heisenberg AFM on a triangular lattice (TAF) by QMC methods have been futile as a consequence of this problem. Because of the experience with this and other frustrated models, we expect that the negative sign problem also invalidates QMC techniques for the system to be studied in this paper. In contrast with the failure of the QMC method, exact diagonalization of the Hamiltonian of the TAF for rather small cells of the lattice has produced the main result for this model: its ground state, contrary to earlier conjectures, was shown to be long-range ordered (see [33]).

According to Lhuillier and her collaborators quantum Heisenberg AFM's at very low temperatures exhibit four distinct kinds of quantum phases.

(1) Semiclassical ordered Néel phases, characterized by long-range order in the spin-spin correlation function, breaking of the SU(2) symmetry, and a gapless spectrum with $\Delta S_z=1$ magnon excitations. The standard example of such order is provided by the Heisenberg AFM on a square lattice in 2D. The theoretical description of such systems using the spin-wave theory (cf. [16]) is quite accurate.

(2) Valence bond crystals (VBC's) (or solids), characterized by long range order in dimer coverings, with prominent examples being the Affleck-Kennedy-Lieb-Tasaki model in 1D [34], or the Heisenberg model on the 2D checkerboard lattice [29,35] (corresponding to a 2D slice of a pyrochlore lattice). VBC's exhibit no SU(2) symmetry breaking, short-range spin-spin correlations, long-range dimer-dimer order and/or order or long-range order of larger $S=0$ plaquettes, and gapped excitations in all S sectors.

(3) Resonating valence bond (RVB) spin liquids (type I), which exhibit a unique ground state, no symmetry breaking of any kind, gapped fractionalized "spinon" excitations, and vanishing correlations in any local order parameter. An example of such a spin liquid is realized in the so-called ring exchange model on the triangular lattice [29].

(4) Resonating valence bond spin liquids (type II), which exhibit no symmetry breaking, no long-range correlations in any local order parameter, and an extraordinary density of states in each total S sector. Numerical work by Dommange *et al.* [36] supports the conjecture of gapless deconfined "spinon" excitations in this scenario. An example of such a spin liquid is believed to be realized by the Heisenberg spin-1/2 model on the kagomé lattice [29,37–43].

The kagomé spin-1/2 antiferromagnet (KAF) seems to be a paradigmatic example of type-II RVB spin liquids, but unfortunately so far no experimental realization of this model has been found among solid-state systems. Only the spin-1 KAF can be realized in solid-state experiments, but that system has a gap to all excitations, i.e., it does not belong to the type-II spin liquids [44]. The physics of the spin-1/2 KAF is, however, not yet fully understood. There are papers that suggest VBC-type order with large unit cells [45].

C. Spinless interacting Fermi gas in a kagomé lattice

We have proposed recently how two realize the trimerized kagomé optical lattices using superlattice techniques, and have studied various kinds of quantum gases in such lattices [11]: (i) a single-component (polarized) Bose gas, (ii) a single-component (polarized) interacting Fermi gas, and (iii) a two-component ("spin"-1/2) Fermi-Fermi mixture. In the subsequent paper [46] we concentrated on the second of the above-mentioned situations and studied the polarized interacting Fermi gas in the trimerized kagomé lattice at the filling $\nu=2/3$. Using the method of exact diagonalization of the Hamiltonian we have shown that the system exhibits an unusual kind of behavior at low temperatures, which has led us to propose a further class of possible behavior of frustrated AFM's:

(5) A quantum spin-liquid crystal, characterized by the long-range Néel type of ordering at low T, gapless spectrum, and anomalously large density of low-energy excitations.

This paper is devoted to the presentation of the details of the theory described in the above-mentioned two Letters Refs. [11,46]. First, we discuss briefly the general properties of interactions in trimerized kagomé lattices as well as the case of a single-component Bose gas in the trimerized kagomé lattice. Then we focus, however, our attention on a trimerized kagomé lattice loaded with a spinless Fermi gas

with nearest-neighbor interaction. At 2/3 filling per trimer such a Fermi gas behaves as a frustrated quantum antiferromagnet, and exhibits quantum spin-liquid crystal behavior. The motivation to study this model is at least fourfold.

(i) In a magnetic field such that the trimerized KAF is driven into the magnetization plateau at 1/3 of the saturation magnetization, the physics of the KAF is described precisely by our model [37–39]. Studying our model will thus exactly shed light on the theory of KAF and, hopefully, on experiments on the KAF.

(ii) Theoretical studies (using exact diagonalization of the Hamiltonian) indicate that the model has the fascinating properties of what we have termed a *quantum spin-liquid crystal*. We expect the behavior observed in this system indeed to be generic for other "multimerized" systems. First of all it is clear that optical methods allow for creating many similar spin models with couplings depending on bond directions. In the simplest case this can be accomplished for a square lattice where one could achieve a "square lattice of small squares," for the triangular lattice to obtain a "triangular lattice of small triangles," etc. One can expect that when such procedures are realized for frustrated systems, this might lead to similar effects as for the kagomé lattice.

(iii) One of the most fascinating possibilities provided by the optical lattices is the possibility of "online" modifications of the lattice geometry. We may go from triangular to kagomé lattice in real time in a controlled way. Trimerization (or generally multimerization) is a different experimental option, and it is highly desirable to explore its consequences. Our model (apart from the model of the Bose gas in the trimerized kagomé lattice) is one of the simplest ones to explore these consequences.

(iv) Last but not least the model is experimentally feasible.

D. Structure of the paper

The paper is organized as follows. In Sec. II we briefly describe the laser arrangement that can be used to create a trimerized optical kagomé lattice. In Sec. II B we first introduce the Hamiltonian that governs the particle dynamics in the lattice: it is a generalized Hubbard model that can be used as a model for bosons, fermions, as well as for boson-fermion or fermion-fermion mixtures in the lattice. We show under which conditions a tight-binding description of the particle dynamics is appropriate in such a lattice, and present results of the calculations of the Hubbard model couplings as a function of parameters of the systems and the degree of trimerization. In Sec. II C we present in some detail the results concerning the physics of a Bose gas in the trimerized kagomé lattice. Here we generalize the results of Ref. [11] obtained in the hard-core boson limit to the case when more than one boson can be present at the same lattice site. Section II D discusses briefly the case of a Fermi-Fermi mixture in the trimerized kagomé lattice.

In Sec. III we start our discussion of the case of 2/3 filling of the trimerized kagomé lattice with spinless fermions. We focus our attention on the case of strong intratrimer and weak intertrimer coupling. First, we discuss various methods of creating an ultracold polarized interacting Fermi gas in an optical lattice (Sec. III A). Then we discuss in detail the intratrimer dynamics. In Sec. III B we show that the low-energy physics of such a gas at 2/3 filling is described by an effective spin-1/2 Hamiltonian with strongly anisotropic couplings. The exchange constant J of this Hamiltonian is proportional to the intertrimer atomic interaction potential which in the low-energy limit can be attractive or repulsive depending on the species of interacting atoms. In favorable cases it can also be manipulated by a magnetic Feshbach resonance. The relation of the model to the Heisenberg spin-1/2 AFM in the kagomé lattice is discussed in Sec. III C. To capture the entire parameter range of the model we investigate the properties of the effective spin Hamiltonian for positive and for negative exchange coupling. We start our investigations of the effective spin model in Sec. III D by looking at its classical and semiclassical behavior. Surprisingly we find that for positive J there exists a very large manifold of degenerate classical ground states (GS's). The semiclassical spin-wave analysis (discussed in Sec. III E and limited to the most symmetric GS's) does favor some of those states but does not give a definite answer concerning the real nature of the quantum ground state. In Sec. IV we present the results of exact diagonalizations of finite cells of the realistic spin-1/2 version of our model. It turns out that even in this extreme quantum limit the ground state of our model exhibits long-range Néel order of the same structure as is found in the classical version. For positive exchange coupling $J>0$ we observe a very high density of low-lying eigenstates of the effective spin model. We associate these low-lying states with the manifold of classical ground states whose degeneracy is lifted by quantum zero-point fluctuations. In the concluding section, Sec. V, we discuss experimental routes toward verification of our results, and detection of the predicted effects. The paper contains two appendices, in which we present the details of the calculations of the couplings in the Hubbard model, and the mean-field theory of the single-component Bose gas, respectively.

II. ATOMIC GASES IN KAGOMÉ LATTICES

A. Creation of optical kagomé lattices

In the following, we consider the atoms confined magnetically or optically in the z direction at $z=0$. The atoms form effectively a 2D system in an optical lattice in the x-y plane. In order to create a kagomé lattice in this plane one can use red-detuned lasers, so that the potential minima coincide with the laser intensity maxima. A perfect triangular lattice can be easily created by two standing waves on the x-y plane, $\cos^2(\mathbf{k}_{1,2}\cdot\mathbf{r})$, with $\mathbf{k}_{1,2}=k\{1/2,\pm\sqrt{3}/2\}$, and an additional standing wave $\cos^2(\mathbf{k}_3\cdot\mathbf{r}+\phi)$, with $\mathbf{k}_3=k\{0,1\}$. The resulting triangles have a side of length $2\pi/\sqrt{3}k$. By varying ϕ the third standing wave is shifted along the y axis, and, in principle, a kagomé pattern could be realized.

Unfortunately, this procedure presents two problems. First, three lasers on a plane cannot have mutually orthogonal polarizations, and consequently undesired interferences between different standing waves occur. This problem has,

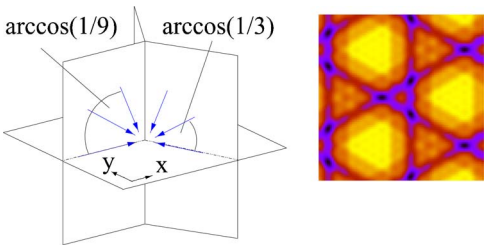

FIG. 1. (Color online) Scheme of the proposed experimental setup. Each arrow depicts a wave vector of a standing-wave laser. The three vertical planes intersect at an angle of 120°. Dark (dark blue in the online version) spots in the right kagomé figure indicate the potential lattice minima.

however, a relatively simple solution: undesired interferences can be avoided by randomizing the relative orientation of the polarization between different standing waves, or by introducing small frequency mismatches, which, however, have to be larger than any other relevant frequencies. The second problem is much more serious, and is caused by the diffraction limit. Let us denote by ξ the ratio between the separation between maxima of the laser intensity (i.e., minima of the resulting optical potential in the case of red-detuned laser beam) and the half width at half maximum. To have a good resolution of the potential minima one needs ξ to be definitely significantly larger than 2. In the case discussed above, however, ξ is only about 4 at $\phi=\pi$ in the ideal kagomé case. Because of that, for any ϕ, the three potential minima forming the kagomé triangles cannot be resolved.

We propose to use the superlattice technique [12] which we briefly describe in the following paragraphs, as a method to generate ideal and trimerized optical kagomé lattices. The proposed experimental setup is schematically shown in Fig. 1. There are three planes of standing-wave laser beams, and the wave vectors of these lasers lie on a plane. In the particular case of Fig. 1, we have three standing waves (a triple) in each plane. The laser fields within each plane are phase locked. A kagomé lattice will be formed by the intensity pattern that results from the sum of the laser intensities of the triples in the x-y plane.

In order to resolve the three potential minima in the unit cell of the kagomé lattice we must use at least two standing waves in each of the three vertical planes shown in Fig. 1. While the wave fields in the same plane must have identical polarizations, the fields in different planes should not interfere. As mentioned above, undesired interference cross terms in the total intensity of the fields can be removed either by randomizing the relative orientations of the polarizations between waves from different planes, or by introducing small frequency mismatches. With this setup consisting of two waves per vertical plane, we obtain the following intensity pattern in the x-y plane:

$$I(\mathbf{r}) = I_0 \sum_{i=1}^{3} [\cos(\mathbf{k}_i \cdot \mathbf{r} + \sigma_i \phi/2) + 2\cos(\mathbf{k}_i \cdot \mathbf{r}/3 + \sigma_i \phi/6)]^2 \quad [\mathbf{r} = (x,y)], \tag{1}$$

where $\sigma_2=-1$ and $\sigma_1=\sigma_3=1$ and the index i enumerates the vertical planes. The pattern formed by the maxima of the intensity $I(\mathbf{r})$ changes between a triangular lattice at $\phi=0$, and trimerized kagomé lattices with varying mesh width for $0<\phi<\pi$, until at $\phi=\pi$ the uniform kagomé lattice is reached. In this limit one obtains the value $\xi\approx 7.6$ at $\phi=\pi$. This is sufficient to create a well-resolved ideal kagomé lattice. Direct inspection shows that in this case a moderately trimerized lattice can also be realized: ξ remains sufficiently large for $5\pi/12 \leqslant \phi \leqslant \pi$, so that the potential minima can still be resolved.

With the additional third beam shown in Fig. 1, a resulting intensity pattern

$$I(\mathbf{r}) = I_0 \sum_{i=1}^{3} [\cos(\mathbf{k}_i \cdot \mathbf{r} + 3\sigma_i \phi/2) + 2\cos(\mathbf{k}_i \cdot \mathbf{r}/3 + \sigma_i \phi/2) + 4\cos(\mathbf{k}_i \cdot \mathbf{r}/9 + \sigma_i \phi/6)]^2 \quad [\mathbf{r} = (x,y)], \tag{2}$$

is obtained. With this arrangement it is possible to transform the optical potential smoothly from an ideal kagomé case into a strongly trimerized lattice. The value of ξ increases in this case to ≈ 14, and remains large in a wide range of angles ϕ.

B. Hubbard Hamiltonian

Depending on the detuning of the laser relative to the resonance frequency of the atoms, either the minima or the maxima of the intensity patterns (1) and (2) form attractive potentials for the atoms. If these potentials are sufficiently strong, the tight-binding approximation holds [47], and the dynamics of the atomic gas can quite generally be described by a Hubbard-type Hamiltonian [2,3]

$$H_{\text{Hubbard}} = -\sum_{\langle ij \rangle} t_{ij}(c_i^\dagger c_j + c_i c_j^\dagger) + \frac{1}{2}\sum_i U n_i(n_i - 1) + \frac{1}{2}\sum_{\langle ij \rangle} U_{ij} n_i n_j. \tag{3}$$

Here $c_i^\dagger$ creates an atom in a Wannier state localized at the lattice site i. Depending on the atomic species the operators $c_i^\dagger, c_i$ represent either fermionic or bosonic creation and annihilation operators. The parameters t_{ij}, U, and U_{ij} of this Hamiltonian are matrix elements of the one-particle Hamiltonian and of the interaction potentials of the gas in the Wannier representation:

$$t_{ij} = \langle \mathcal{W}_i | H_0 | \mathcal{W}_j \rangle, \tag{4}$$

where H_0 is the one-particle Hamiltonian,

$$H_0 = -\frac{\hbar^2}{2m}\Delta + v(\mathbf{r}), \tag{5}$$

with the one-particle potential $v(\mathbf{r}) \propto \pm I(\mathbf{r})$–see Eqs. (1) and (2). The sign depends on the detuning. For the Bose gas interacting via short-range van der Waals forces, the scattering at low energies occurs via the s-wave channel, and is adequately described by the zero-range potential, so that

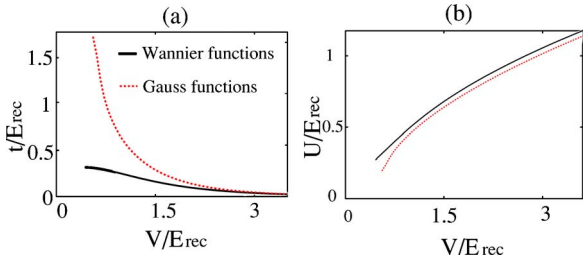

FIG. 2. (Color online) Couplings for a perfect kagomé lattice obtained using the Gaussian approximation (dotted lines) and using the exact Wannier functions (solid lines). (a) Hopping matrix elements; (b) contact interaction in units of E_{rec}.

$$U = g_{2\mathrm{D}} \int d^2x |\mathcal{W}_i(\mathbf{r})|^4, \tag{6}$$

whereas

$$U_{ij} = g_{2\mathrm{D}} \int d^2x |\mathcal{W}_i(\mathbf{r})|^2 |\mathcal{W}_j(\mathbf{r})|^2, \tag{7}$$

where the coupling $g_{2\mathrm{D}}=4\pi\hbar^2 a_s/mW$ with m the atomic mass, and with W the effective transverse width of the 2D lattice in the z direction. In the case of polarized fermions U vanishes, since s-wave scattering is not possible due to the Pauli principle. Nearest neighbor interactions, on the other hand, are possible, and in the case that they are due to dipolar forces (cf. [48]) or similar long-range forces the couplings become

$$U_{ij} \sim \int d^2x\, d^2x' |\mathcal{W}_i(\mathbf{r})|^2 V(\mathbf{r}-\mathbf{r}') |\mathcal{W}_j(\mathbf{r}')|^2, \tag{8}$$

where $V(\mathbf{r})$ is the interparticle potential. Obviously, the same expression holds also for bosons interacting via the potential $V(\mathbf{r})$. The Hubbard Hamiltonian (3) does not necessarily describe the physics of bare particles; it may equally well describe the physics of composite objects, such as, for instance, composite fermions that arise in the analysis of Fermi-Bose mixtures in the lattice in the strong-interaction limit [21]. The nearest-neighbor interactions and tunnelings are induced by the original hopping of bare fermions and bosons, and the corresponding values of t_{ij} and U_{ij} have to be calculated from the bare couplings following the lines of Ref. [21].

In this paper we present explicit results for the tunneling matrix elements t_{ij} and the interaction strengths U and U_{ij} in the case of zero-range potential—expressions (4), (6), and (7). With this aim we need to determine the Wannier functions $\mathcal{W}_i(\mathbf{r})$ for kagomé-type lattices. The method by which this task can be accomplished is presented in detail in Appendix A.

For the ideal kagomé lattice we have successfully generated the exact Wannier functions, and calculated the couplings accordingly. These results were then compared with the results of the variational method employing a Gaussian ansatz (for details see Appendix A). Figure 2 compares the results calculated with Wannier functions and the Gaussian ansatz. For moderately strong potentials, say larger than two times the recoil energy E_{rec}, the Gaussian approximation becomes appropriate, giving errors less than 50%. For sufficiently high potential amplitudes above $5E_{\mathrm{rec}}$, the results obtained with the Gaussian approximation become practically indistinguishable from the exact Wannier results.

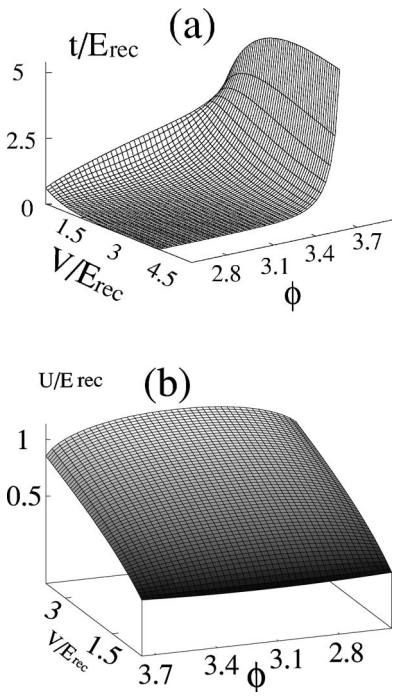

FIG. 3. Couplings for a trimerized lattice obtained with a Gauss function: (a) intertrimer ($\phi \leqslant \pi$) and intratrimer ($\phi \geqslant \pi$) hopping matrix elements; (b) contact interaction terms in units of E_{rec}.

Generating well-localized Wannier functions in the trimerized lattices is a difficult task. For this reason, guided by the results for the ideal kagomé lattice, we have limited ourselves here only to the results of the Gaussian approximation. Figure 3 shows the hopping and interaction matrix elements depending on the trimerization angle. The perfect kagomé lattice can be obtained by setting $\phi=\pi$. As expected, trimerization does not affect the on-site interactions very strongly, but does change the tunneling rates by orders of magnitude. Already a relatively moderate trimerization introduces large difference between the inter- and intratrimer hopping elements.

C. Bose gas in the trimerized kagomé lattice

As we mentioned in Sec. I, in the present paper our main focus will be on a gas of spinless fermions on the trimerized kagomé lattice at 2/3 filling. Other cases of interest which we will briefly discuss now include a Bose gas and a Fermi-Fermi mixture in this lattice.

In order to facilitate the calculations, we add to the Hamiltonian (3) a term of the form $-\mu\Sigma_i n_i$, where μ is the chemical potential, that controls the average particle number of the system. Working with a fixed number of particles is possible, but technically very tedious. In the trimerized kagomé lattice, the couplings t_{ij} take the values t, t' for intra- and intertrimer hopping, respectively. We set also $U_{ij}=V$ and $=V'$, for intra- and intertrimer interactions.

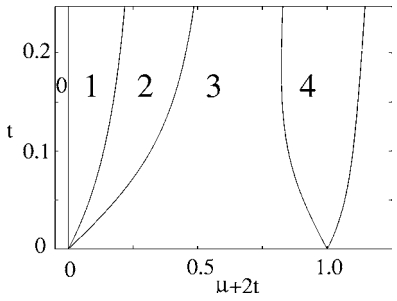

FIG. 4. Mott phases (denoted by the corresponding particle numbers per trimer) of the state with lowest energy in the $t-(\mu+2t)$ plane for zero intertrimer hopping $t'=0$.

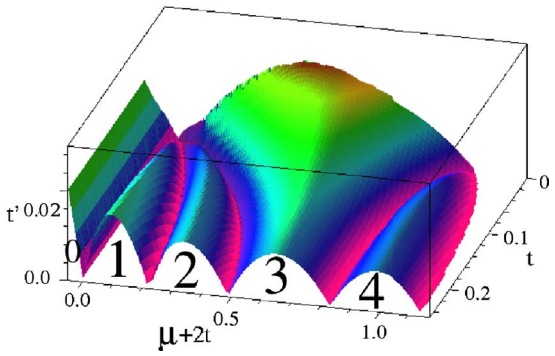

FIG. 5. (Color online) Phase boundaries between Mott and superfluid phases in parameter space of the hopping elements t,t' and the chemical potential μ. Below the loops the state is in a Mott phase, where the number of bosons per trimer is displayed in the diagram.

In Ref. [11] we have considered the limiting case of hard-core bosons, when U was much larger than any other energy scale, i.e., two bosons were not allowed at the same site. We have shown then that in the strongly trimerized case ($t',V' \ll V<t$) the system will enter a trimerized Mott phase with the ground state corresponding to the product over (independent) trimers. Depending on the particular value of $\bar{\mu} \equiv(\mu-V)/(2t+V)$ we may have 0 ($\bar{\mu}<-1$), 1 ($-1\leqslant\bar{\mu}<0$),2 ($0\leqslant\bar{\mu}<1$), or 3 ($1\leqslant\bar{\mu}$) bosons per trimer, i.e., filling factors $\nu=0,1/3,2/3$, or 1 boson per site. For fractional filling, the atoms within a trimer minimize the energy forming a so-called W state [49]: $|W\rangle=(|001\rangle+|010\rangle+|100\rangle)/\sqrt{3}$ for $\nu=1/3$, and $|W\rangle=(|110\rangle+|101\rangle+|011\rangle)/\sqrt{3}$ for $\nu=2/3$. It is worth noticing that W states themselves have interesting applications for quantum information theory (cf. [50]).

Generalizing the Landau mean-field theory of Ref. [19], we have obtained the phase diagram in the $\bar{t}'\equiv t'/(2t+V)$ and $\bar{\mu}$ plane with characteristic lobes describing the boundaries of the Mott phases, given by $\bar{t}'=(|\bar{\mu}|-1)/2$ for $|\mu|\geqslant 1$, and $\bar{t}'=(3/2)|\bar{\mu}|(1-|\bar{\mu}|)/(4-|\bar{\mu}|)$ for $|\mu|<1$. Observations of this Mott transition require temperatures T of the order of t', i.e., smaller than t and V. Assuming that U is of the order of a few recoil energies [3], this requires T to be in the range of tens of nanokelvin. The results for $t<V$ are qualitatively similar.

In this paper we present a method to generalize these results to the case when the bosons are not necessarily hard core, i.e., U may be comparable with t. For simplicity we set $U_{ij}=0$, so that the Hamiltonian is still described by the three parameters t and t' for intra- and intertrimer hopping, and U for the on-site interactions. Obviously, for vanishing intertrimer hopping, $t'=0$, the system is in a Mott insulating state with a fixed number of particles per trimer. The corresponding Mott states are displayed in the phase diagram in the $t-(\mu+2t)$ plane in Fig. 4. As t' is increased the system undergoes a phase transition into a superfluid state. To obtain the phase diagram for this transition, Fig. 5, we have used a generalization of the Landau mean-field approach of Fisher *et al.* [19,51,52], also investigated in [53]. Details of the method can be found in Appendix B. In our calculations we have confined ourselves to values of the chemical potential such that the particle number per trimer does not exceed four. In Fig. 5, further lobes with higher particle numbers will occur along the μ axes for higher values of μ than those shown. Instead of calculating the so-called superfluid order parameter $\psi=\langle b_i\rangle=\langle b_i^\dagger\rangle$ self-consistently, a fully analytical expressions describing the boundaries in Fig. 5 can be obtained, as is shown in Appendix B. We mention that by using a cell strong-coupling perturbative expansion [54] the phase boundary can be obtained with relatively little numerical effort with the accuracy of a quantum Monte Carlo simulation.

D. Fermi-Fermi mixture at 1/2 filling in the trimerized kagomé lattice: Spin-1/2 Heisenberg antiferromagnet

For a fermion-fermion mixture, instead of the extended Hubbard model described by the Hamiltonian (3) which includes nearest-neighbor interactions U'_{ij}, it is more appropriate to consider the Hamiltonian with on-site interactions only:

$$H_{FF}=-\sum_{\langle ij\rangle} t_{ij}(f_i^\dagger f_j+\tilde{f}_i^\dagger \tilde{f}_j+\text{H.c.})+\sum_i V n_i \tilde{n}_i. \tag{9}$$

Here f_j and $\tilde{f}$ denote the fermion annihilation operators for the two species, and $n_i,\tilde{n}_i$ are the corresponding occupation operators. The tunneling matrix elements are $t_{ij}=t$ for intratrimer and $t_{ij}=t'$ for intertrimer nearest-neighbor tunneling. H_{FF} is then the spin-1/2 Hubbard model. In the strong-coupling limit, $t,t'\ll V$, this model can be transformed into the t-J model [16] which reduces to the spin-1/2 Heisenberg model for half filling,

$$H_{FF}\rightarrow H^{Heisenberg}=J\sum_{\langle ij\rangle_{intra}} \mathbf{S}_i\cdot\mathbf{S}_j+J'\sum_{\langle ij\rangle_{inter}} \mathbf{S}_i\cdot\mathbf{S}_j, \tag{10}$$

where $J=4t^2/V$, $J'=4t'^2/V$, and $\mathbf{S}=(S^x,S^y,S^z)$ with $n-\tilde{n}=2S^z$, $f^\dagger\tilde{f}=S^x+iS^y$, and $\tilde{f}^\dagger f=S^x-iS^y$. It is exactly the model described by $H^{Heisenberg}$ that has been studied by Mila and Mambrini [38,39] in their effort to gain a physical understanding for the low-lying part of the spectrum of the kagomé antiferromagnet. The physics of this model is very interesting. In the trimerized case, it seems to be clear that the system qualifies as a RVB spin liquid of the second type. The large density of singlet and triplet excitations can be

predicted quite well by analyzing the number of "relevant" dimer coverings of the trimerized lattice. The singlet-triplet gap, if it exists at all, is extremely small. All of these findings have so far no experimental confirmation. Experiments on this system are thus highly desirable, and we hope that ultracold atoms will allow their realization.

III. SPINLESS INTERACTING FERMI GAS IN THE TRIMERIZED KAGOMÉ LATTICE AT 2/3 FILLING

A. Experimental realization

Before we start to discuss the properties of the spinless interacting Fermi gas in the trimerized kagomé lattice, we shall first discuss the possibilities of preparing such a system. There are essentially two ways of achieving this goal. First, we may consider an ultracold gas of fermions that interact via dipole-dipole forces. Bose-Einstein condensation of a dipolar gas of chromium atoms has been recently achieved by the group of Pfau [55]. The (magnetic) dipolar interactions in chromium are significant, but not very strong. There are many ongoing experiments, however, aimed at the creation of ultracold gases of heteronuclear molecules, that could carry electric dipole moments of the order of a debye (cf. [56]). The observation of physics described in this paper using heteronuclear molecules with such strong dipoles should be possible already at temperatures $T \simeq 100$ nK.

Another possibility of creating an interacting Fermi gas is to use the gas of composite fermions that appears in the low-temperature behavior of Fermi-Bose mixtures in the limit of strong Bose-Bose and Bose-Fermi interactions. As we have mentioned above the physics of such composite fermions is described also by an extended Hubbard model, in which the couplings result from virtual tunneling processes involving bare fermions and bosons. In this case the observation of the low-temperature physics requires achieving low but not unrealistic temperatures $T \simeq 10$–50 nK (cf. Ref. [22]).

The low-energy states may be prepared by employing adiabatic changes of the degree of trimerization of the lattice. For instance, one can start with a completely trimerized lattice; then the filling $\nu=2/3$ may be achieved by starting with $\nu=1$ and by eliminating one atom per trimer using, for instance, laser excitations. One can then increase t' and U' slowly on a time scale larger than $1/J$ ($\simeq$seconds). Alternatively, one could start with $\nu \simeq 2/3$ in the moderately trimerized regime. As in Ref. [3], the inhomogeneity of the lattice due to the trapping potential would then allow one to achieve the Mott state with $\nu=2/3$ per trimer in the center of the trap. Nearly perfect 2/3 filling can be reached by loading a BEC of molecules formed by two fermions into a triangular lattice, generating a MI state adiabatically, transforming the lattice to a trimerized kagomé one, "dissociating" the molecules by changing the scattering length to negative values, and finally optically pumping the atoms into a single internal state. Preparing $\nu=2/3$ might involve undesired heating (due to optical pumping) which can be overcome by using laser or phonon cooling afterward (cf. [57]). Note that the imperfections of ν can be described by a "t-J" kind of model, and are of interest themselves.

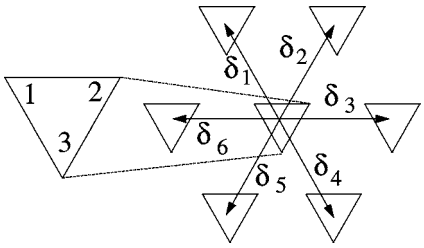

FIG. 6. The vectors $\boldsymbol{\delta}_i$, $i=1, \ldots, 6$, pointing from the center of a given trimer to the centers of neighboring trimers. Numbering of the sites of the trimers is shown in the triangle on the left.

B. Effective spin model

The spinless Fermi gas in the trimerized kagomé lattice is appropriately described by the Fermi-Hubbard Hamiltonian

$$H_{FH} = -\sum_{\langle ij \rangle} (t_{ij} f_i^\dagger f_j + \text{H.c.}) + \sum_{\langle ij \rangle} U_{ij} n_i n_j - \sum_i \mu n_i, \quad (11)$$

where t_{ij} and U_{ij} take the values t and U for intratrimer bonds and t' and U' for intertrimer bonds. μ is the chemical potential, and $n_i = f_i^\dagger f_i$ are the occupation numbers with $f_i, f_i^\dagger$ the fermion annihilation and creation operators. In the following we denote the sites of each trimer by 1, 2, 3 in the clockwise sense as shown in Fig. 6.

In this section it is our aim to derive from the Hamiltonian (11) an effective spin Hamiltonian that captures in the strongly trimerized limit, $t', U' \ll t < U$, the low-energy physics the model (11).

The intratrimer part of the Hamiltonian H_{FH} is diagonalized by introducing instead of the local fermion modes f_1, f_2, and f_3 the symmetric mode $f=(f_1+f_2+f_3)/\sqrt{3}$ and the left and right chiral modes $f_\pm = (f_1 + z_\pm f_2 + z_\pm^2 f_3)/\sqrt{3}$ with $z_\pm = \exp(i 2\pi/3)$:

$$H_{FH}^{intra} = -3tn + t\bar{n} + \frac{U}{2}(\bar{n}^2 - \bar{n}) - \mu\bar{n}, \quad (12)$$

where $n = f^\dagger f$ and where $\bar{n} = n + f_+^\dagger f_+ + f_-^\dagger f_-$ is the total number of fermions in the trimer. In the strongly trimerized limit the number of fermions is identical in each trimer. It is controlled by the chemical potential: for $U+J < \mu < 2U+J$ there are two particles in each trimer; one of them occupies the symmetric state $|1\rangle = f^\dagger|0\rangle$, while the second one occupies either one of the chiral states $|1\pm\rangle = f_\pm^\dagger|1\rangle$.

In the intertrimer part of the Hamiltonian H_{HF}, Eq. (11), we neglect the hopping term, $-\Sigma_{\langle \alpha i, \beta j \rangle} t' (f_{\alpha,i}^\dagger f_{\beta,j} + \text{H.c.})$ ($\alpha, \beta = 1,2,3$ referring to intratrimer indices and i numbering trimers), since any real (first-order) hopping process leads to an excited state whose energy is $O(U)$ higher than the ground-state energy and since second-order (virtual) hopping processes yield contributions which are small, of order t'^2/U. Then, the inter-trimer part of H_{HF} reduces to

$$H_{HF}^{inter} = \frac{U'}{2} \sum_i (n_{1,i} n_{3,i+\boldsymbol{\delta}_1} + n_{2,i} n_{3,i+\boldsymbol{\delta}_2} + n_{2,i} n_{1,i+\boldsymbol{\delta}_3} + n_{3,i} n_{1,i+\boldsymbol{\delta}_4} + n_{3,i} n_{2,i+\boldsymbol{\delta}_5} + n_{1,i} n_{2,i+\boldsymbol{\delta}_6}). \quad (13)$$

Here, $\boldsymbol{\delta}_\nu$, $\nu = 1, \ldots, 6$, denote the six vectors pointing from the

central triangle to the six neighboring triangles; see Fig. 6.

Next we express the occupation numbers $n_{\alpha,i}, \alpha=1, 2, 3$, in terms of the fermion operators f, $f_\pm$ (we suppress the site index):

$$n_1 = \frac{1}{3}[\bar{n} + (f_+^\dagger + f_-^\dagger)f + f^\dagger(f_+ + f_-) + \tau^x], \tag{14}$$

$$n_2 = \frac{1}{3}[\bar{n} + (z_+ f_+^\dagger + z_- f_-^\dagger)f + f^\dagger(z_- f_+ + z_+ f_-) + \cos(2\pi/3)\tau^x + \sin(2\pi/3)\tau^y], \tag{15}$$

$$n_3 = \frac{1}{3}[\bar{n} + (z_+^2 f_+^\dagger + z_-^2 f_-^\dagger)f + f^\dagger(z_-^2 f_+ + z_+^2 f_-) + \cos(2\pi/3)\tau^x - \sin(2\pi/3)\tau^y]. \tag{16}$$

Here, the (pseudo)spin operators $\hat{\tau}^x := \frac{1}{2}(f_+^\dagger f_- + f_-^\dagger f_+)$, $\hat{\tau}^y := -(i/2)(f_+^\dagger f_- - f_-^\dagger f_+)$ connect the right- and left-handed chiral fermion states. Inserting expressions (14)–(16) into H_{HF}^{inter}, Eq. (13), yields bilinear terms in $\hat{\tau}^x, \hat{\tau}^y$, linear terms in $\hat{\tau}^x$ and $\hat{\tau}^y$, bilinear terms in $f^\dagger, f$ and linear terms in $f^\dagger$ and f. Since none of these terms changes the total number of fermions in any of the trimers, we may set $\bar{n}=2$ in the resulting expression for H_{HF}^{inter}. However, terms containing the annihilation operator f promote the fermion in the symmetric state of a given trimer into the nonoccupied chiral state of the same trimer. A glance at H_{FH}^{intra}, Eq. (12), shows that the energy of this excited state is $O(t)$ above the ground-state energy. Thus, on account of analogous arguments as were given above for the neglect of the hopping term of H_{HF}^{inter}, we also neglect all terms containing the operators $f^\dagger, f$. The linear terms in $\hat{\tau}_i^x, \hat{\tau}_i^y$ sum to zero in the sum over the sites i so that we arrive at the following effective intertrimer Hamiltonian (we omit an irrelevant constant):

$$H_{eff} = \frac{J}{2}\sum_{i=1}^{N}\sum_{\nu=1}^{6} \hat{\tau}_i(\phi_{i,\boldsymbol{\delta}_\nu})\hat{\tau}_{i+\boldsymbol{\delta}_\nu}(\tilde{\phi}_{i,\boldsymbol{\delta}_\nu}). \tag{17}$$

Here, i are the sites of a triangular lattice of N sites on which the trimers are located, $J=4U'/9$, and the vectors $\boldsymbol{\delta}_\nu$, $\nu=1$, …, 6, are the same as in Fig. 6. In Eq. (17), $\hat{\tau}_i(\phi) = \cos(\phi)\hat{\tau}_i^x + \sin(\phi)\tau_i^y$ and $\phi_{i,\boldsymbol{\delta}_1} = \phi_{i,\boldsymbol{\delta}_6} = 0$, $\phi_{i,\boldsymbol{\delta}_2} = \phi_{i,\boldsymbol{\delta}_3} = 2\pi/3$, $\phi_{i,\boldsymbol{\delta}_4} = \phi_{i,\boldsymbol{\delta}_5} = -2\pi/3$, $\tilde{\phi}_{i,\boldsymbol{\delta}_1} = \tilde{\phi}_{i,\boldsymbol{\delta}_2} = -2\pi/3$, $\tilde{\phi}_{i,\boldsymbol{\delta}_3} = \tilde{\phi}_{i,\boldsymbol{\delta}_4} = 0$ and $\tilde{\phi}_{i,\boldsymbol{\delta}_5} = \tilde{\phi}_{i,\boldsymbol{\delta}_6} = 2\pi/3$.

C. Effective spin model: Relation to kagomé antiferromagnet

At this point it seems appropriate to briefly discuss the connection between the effective Hamiltonian H_{eff} derived here as model for the dynamics of fermionic atoms on a trimerized kagomé lattice and the model Hamiltonian that has been derived by Subrahmanyam [37] and has later been employed by Mila and Mambrini [38,39] to explain the origin of the high density of low-lying singlets of the Heisenberg antiferromagnet on the kagomé lattice. Mila considers the spin-1/2 Heisenberg model on the trimerized kagomé lattice with a strong intratrimer coupling J and a weak intertrimer coupling J'. In the lowest-order perturbation expansion with respect to J' he arrives at the effective Hamiltonian

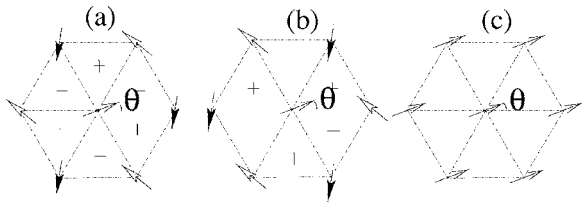

FIG. 7. (a) Classical ground-state configuration for $J<0$ (configuration A). (b), (c) Classical ground-state configurations for $J>0$ (configuration B and ferromagnetic configuration). The $+,-$ signs denote the chirality of the triangular plaquettes (19).

$$H_{eff}^{trim\ kag} = \frac{J'}{18}\sum_{\langle ij\rangle} H_{ij}(S_\nabla)H_{ij}(\tau), \tag{18}$$

where $H_{ij}(S_\nabla) = \mathbf{S}_{\nabla i}\mathbf{S}_{\nabla j}$ and where $H_{ij}(\tau)$ is that member of our model H_{eff} that is associated with the bond ij. The operator $\mathbf{S}_{\nabla i}$ acts on the total spin of the trimer at site i, the trimers form a triangular lattice. In the derivation $H_{eff}^{trim\ kag}$ the Hilbert space of the three $S=1/2$ spins of the individual trimers has been restricted to the subspace of total spin-1/2 states. The four states of this subspace can be be specified by the z component of their total spin and by two (spin) chiralities. The Heisenberg type Hamiltonian $H_{ij}(S_\nabla)$ acts on the two spin states of the trimers at sites i and j; $H_{ij}(\tau)$ acts on their chiralities. Obviously, $H_{eff}^{trim\ kag}$ turns into our model Hamiltonian H_{eff}, if the trimer spins $S_{\nabla i}^z$ are fully polarized, e.g., $S_\nabla^z = 1/2$ for all i. This state can be reached by applying a sufficiently strong magnetic field to the original trimerized kagomé AFM such that the total magnetization reaches 1/3 of the saturation magnetization, i.e., a magnetic field that establishes the 1/3 magnetization plateau.

D. Effective spin model: Classical aspects

As is obvious from the derivation of the Hamiltonian (17), only its $\tau=1/2$ quantum version can serve as a realistic effective model for the atomic Fermi gas in the trimerized kagomé lattice. Nevertheless, for orientational purposes it is useful to first consider this model in the classical limit and to also calculate its excitation spectrum in the semiclassical approximation, i.e., in the linear spin-wave (LSW) approximation. We first describe the symmetries of the model Eq. (17).

We have found that this model is not only translationally invariant, but is also invariant under the point group of order 6, $Z_6 = Z_3 \cdot Z_2$, where the generator of Z_3 (order 3) is the combined rotation of the lattice by the angle $4\pi/3$ and of the spins by the angle $2\pi/3$ around the z axis, while the generator of Z_2 (order 2) is the spin inversion in the x-y plane, $\hat{\tau}_i^x \to -\hat{\tau}_i^x, \hat{\tau}_i^y \to -\hat{\tau}_i^y$. The model possesses *no* continuous spin rotational symmetry and the lines bisecting the angle between two adjacent lattice directions of the triangular lattice are *not* mirror lines.

In Figs. 7(a)–7(c) we show the three ordered classical states with small unit cells on the triangular lattice that are compatible with this point group symmetry: a ferromagnetic

state and two 120° Néel states labeled A and B which differ by the distributions of the chiralities χ over the cells of the lattice as indicated by + and − signs. For an elementary cell of the triangular lattice whose corners are labeled i,j,k in the counterclockwise sense, χ is defined as [58]

$$\chi_{ijk} = (\tau_i^x \tau_j^y - \tau_i^y \tau_j^x) + (i,j \to j,k) + (j,k \to k,i). \quad (19)$$

χ is positive (negative) if the spin turns in the counterclockwise (clockwise) sense as one moves around a triangular cell in the counterclockwise sense. Because of the lack of mirror symmetry mentioned above it is not surprising that the two Néel states have different energies: $E^A_{\text{class}} = \frac{3}{2}\tau^2 JN, E^B_{\text{class}} = -\frac{3}{4}\tau^2 JN$. Here, N is the number of sites and the superscripts A and B correspond to the labels of the Néel states in Figs. 7(a) and 7(b).

More surprisingly the ferromagnetic state is found to be degenerate with the Néel state B in the classical limit, $E^{\text{ferro}}_{\text{class}} = E^B_{\text{class}}$. Furthermore, as is indicated by the angle θ in Figs. 7(a) and 7(b) the classical energies of the three structures do not depend on their direction relative to the lattice directions. In summary, in the classical approximation the Néel state A is the ground state of model Eq. (17) for negative coupling $J<0$, while for positive J there are at least two classically degenerate GS's, the Néel state B and the ferromagnetic state.

In fact, we have performed a numerical analysis of the 12-spin cell by fixing the direction of every spin to $n\pi/3$ with $n=0,\cdots,5$, so that there were 6^{12} classical spin configurations. This analysis has revealed that for $J<0$ there are six ground states, each of them exhibiting the Néel order of type A (the sixfold degeneracy comes from a Z_6 symmetry of our model). The results are dramatically different in the $J>0$ case, where we have found in total 240 degenerate classical GS's, among which the pure Néel states of type B and ferromagnetic states sum up to a small fraction. For an illustration, see Fig. 8 where two ordered GS's with very large unit cells [Figs. 8(b) and 8(d)] together with their parent states [Figs. 8(a) and 8(c)] are presented. As will be seen below, the large number of degenerate classical GS's may find its analog in a large density of low-lying excitations of the quantum version of Eq. (17).

E. Effective spin model: Spin-wave theory

The linear spin-wave expansion around the ferromagnetic GS based on the Holstein-Primakoff expansion [16] of the spin operators $\hat{\tau}^x, \hat{\tau}^y$ is straightforward. The spin-wave frequency depends on the direction θ of the magnetization relative to the main lattice directions of the triangular lattice [see Fig. 7(c)]:

$$\omega^{\text{ferro}} = \frac{3}{2} J\tau \sqrt{1 - \frac{4}{3} f(\mathbf{q},\theta)},$$

where

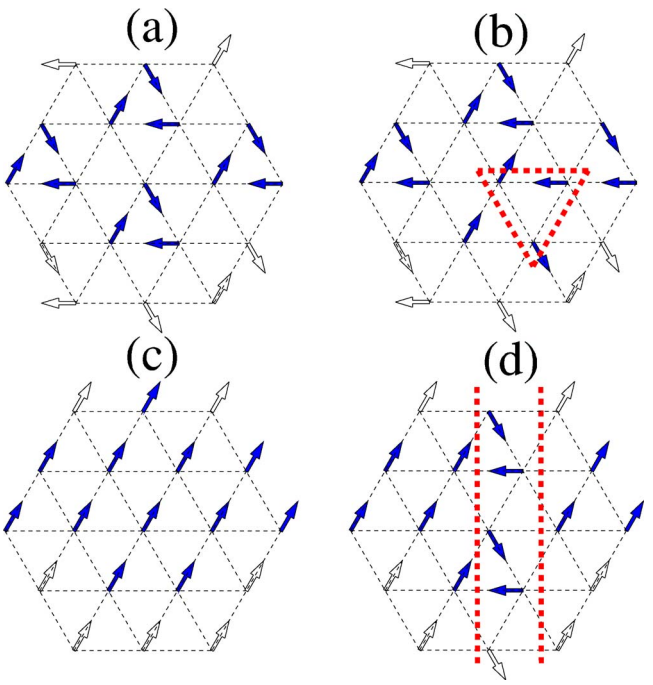

FIG. 8. (Color online) N=12 spin cell: (a) Configuration B; (b) Localized defect in configuration B marked by the triangular contour. (c) Ferromagnetic configuration; (d) Line defect in ferromagnetic configuration. The open arrows present spins that do not belong to the 12-spin cell. Their orientations are determined by the boundary conditions of the cell.

$$f(\mathbf{q},\theta) = -\sin\left(\frac{2\pi}{3} + \theta\right)\sin\theta\cos(\mathbf{q}\cdot\boldsymbol{\delta}_1) + \sin\left(\frac{2\pi}{3} + \theta\right)\sin\left(\frac{2\pi}{3} - \theta\right)\cos(\mathbf{q}\cdot\boldsymbol{\delta}_2) + \sin\left(\frac{2\pi}{3} - \theta\right)\sin\theta\cos(\mathbf{q}\cdot\boldsymbol{\delta}_3).$$

The quantum correction to the GS energy, δE^{ferro}, is found as

$$\delta E^{\text{ferro}}(\theta) = -\frac{3}{4} J\tau + \frac{1}{2N}\sum_{\mathbf{q}} \omega^{\text{ferro}}(\mathbf{q},\theta). \quad (20)$$

(In the above expression and till the end of this section all expressions for energies present energies per site.) Evaluating the sum in this expression one finds that δE^{ferro} is minimal, if θ takes one of the six values $\pi n/3, n=0, \ldots, 5$. Thus, owing to the lowest-order quantum corrections to the GS energy, the magnetization of the ferromagnetic state locks in on one of the directions of the triangular lattice, i.e., the ferromagnetic GS becomes sixfold degenerate in accordance with the order of the point group of our model, Eq. (17). With inclusion of these lowest-order quantum corrections the GS energy for the preferred values of θ is given by

$$E^{\text{ferro}} = -\frac{3}{4} J[\tau(\tau+1) - 0.901\tau]. \quad (21)$$

In order to obtain the spin-wave frequencies for the two 120° structures we closely follow the method devised by Jolicœur

and Le Guillou [59] for the semiclassical treatment of the Heisenberg AFM on the triangular lattice. Since the unit cells of both Néel structures A and B contain three sites one obtains in both cases three surfaces of spin wave frequencies in the magnetic Brillouin zone (BZ), ω_α^A and ω_α^B, $\alpha=1,2,3$. As for the ferromagnetic state, the values of these frequencies depend on the angle θ between these structures and the main directions of the triangular lattice, and hence the quantum corrections to the GS energies of the states A and B, δE^A and δE^A, depend on θ. For general θ the expressions for the spin-wave frequencies are rather complicated. However, by considering small deviations of θ from the the values $\pi n/3$ we find that as in the ferromagnetic case the quantum corrections $\delta E^A(\theta), \delta E^B(\theta)$ are minimal for $\theta=\pi n/3, n=0, \ldots, 5$, i.e., the Néel structures A and B also lock in on the directions of the triangular lattice and hence both Néel states are sixfold degenerate. Remarkably, for the structure B all three branches of spin-wave frequencies are dispersionless with the lowest branch consisting of $N/3$ zero modes, $\omega_1^B(\mathbf{q})=0$ for all $\mathbf{q}$ in the magnetic BZ. This is reminiscent of the Heisenberg model on the kagomé lattice (HAK) for which one also finds $N/3$ zero-frequency spin-wave modes. The nature of these zero modes is, however, quite different for the two models. While they correspond to simultaneous out-of-plane rotations of six-spin clusters in the HAK [60], they represent rigid in-plane rotations of the three spins on the corners of an elementary triangle in our model (17).

Since it is of interest, we also note here the expression for the GS energy of the state B after the lowest quantum correction has been included:

$$E^B = -\frac{3}{4}J[\tau(\tau+1) - 1.48\tau]. \tag{22}$$

Comparison of Eqs. (21) and (22) shows that quantum fluctuations lift the degeneracy of the purely classical states. In this semiclassical approach it appears that the ferromagnetic state is the GS. We recall, however, that there is a very large manifold of classical GS's. In this manifold there may well be states that have lower energies than the two states that we have compared here.

IV. NUMERICAL RESULTS

A. Numerical method

To describe the physics of spinless fermions on a trimerized optical kagomé lattice at filling 2/3 we need to consider the model (17) for spin $\tau=1/2$, i.e., in the extreme quantum limit. Questions to be answered for this case are the following. (i) Is the GS of the model (17) an ordered state or is it a spin liquid either of type I, i.e., a state without broken symmetry, with exponentially fast decaying spin pair correlations, and a gap to the first excitation, or of type II, i.e., a kagomé-like GS, again without broken symmetry, with extremely short-ranged correlations, but with a dense spectrum of excitations adjacent to the GS. (ii) What are the thermal properties of our system? After all, the model can only be realized at finite, albeit low, temperatures.

To find answers to these questions we have performed exact diagonalizations (ED's) of the the Hamiltonian (17) for cells of $N=12$, 15, 18, 21, and 24 sites using ARPACK routines [61]. The sizes of systems that can be studied by ED are restricted by the amount of memory space that is required for storing the nonzero matrix elements. To reduce this requirement we block-diagonalized the Hamiltonian (17) by exploiting its invariance under N-fold translations. It allowed us to reduce the problem of diagonalization of a $2^N \times 2^N$ matrix to N *independent* diagonalizations of matrices of size $\sim 2^N/N \times 2^N/N$. This simplification not only lowers the memory requirements but also greatly reduces the time of calculation, especially when a large number of excited eigenstates is of interest.

Nevertheless, ED of this Hamiltonian remains a demanding task, as in contrast to SU (2)-invariant spin models the Hilbert space of the Hamiltonian (17) cannot be separated into subspaces of states with fixed total spin and total z component of the spin. Because of this last circumstance we had to limit our study to systems of at most 24 spins. Fortunately, our results for 21 and 24 spins show qualitative and quantitative resemblance. Therefore we regard them as representative for larger systems too. In presenting our results we shall mainly confine ourselves to the two largest systems, since the results for smaller systems suffer from strong finite-size effects. We remark that only the 12- and the 21-site cells can be chosen such that these systems possess the full point-group symmetry of the infinite lattice. The lack of this symmetry for the 15- and the 18-site cells adds to the large finite-size effects observed in the results for these cells.

B. Ground-state and low-temperature properties

For $J<0$, i.e., for attractive interaction U' between fermions on nearest-neighbor trimers, the highest levels of H_{eff}/J and the corresponding eigenstates are physically most relevant. As will be seen below these levels are well separated from each other so that we only need to calculate a few of them. The situation is drastically different in the case $J>0$, where we need the low-lying states of H_{eff}. It turns out that there is an abundance of such low-lying states. In this respect the spectrum of H_{eff} is reminiscent of the spectrum of the Heisenberg Hamiltonian on the kagomé lattice [40,42]. The answer to the question of whether there is long-range order in our model (17) is found in Tables I and II, where we show our numerical results for the spatial spin-spin correlations for the $J<0$ and $J>0$ cases, respectively. The cells to which these tables refer are shown in Figs. 9(a)–9(c).

Let us first consider the case $J<0$, Table I. We have not done a systematic finite-size analysis for these correlations. However, comparing the data for the quantum $\tau=1/2$ systems with the classical correlations there can be little doubt that in its GS the system orders in the planar 120°Néel structure. The smallness of the out-of plane correlations lends further support to this conclusion. We have also calculated the expectation values of the chirality χ_{ijk}, Eq. (19), in the GSs of the 12- and of the 21-site cell and have found perfect agreement with the pattern of positive and negative chiralities of the classical configuration, Fig. 7(a). Apparently, for $J<0$ quantum fluctuations have a rather weak effect on the GS properties of our model (17).

TABLE I. Spin-spin correlations $\langle \hat{\tau}_0^x \hat{\tau}_j^x + \hat{\tau}_0^y \hat{\tau}_j^y \rangle$ for $J<0$. In the last row the τ^z-τ^z correlations for $N=21$ are also shown (numbers in parentheses). Owing to the Z_6 symmetry of the Hamiltonian (17) the correlations depend only on the distance d from the central site 0 (see Fig. 9).

	1st neighbors $d=1$	2nd neighbors $d=\sqrt{3}$	3rd neighbors $d=2$	4th neighbors $d=\sqrt{7}$
Classical	−0.125	0.25	−0.125	−0.125
$N=12$	−0.137	0.251	−0.125	
$N=21$	−0.134	0.237	−0.117	−0.116
	(−0.029)	(−0.004)	(−0.004)	(−0.003)

For the case $J>0$ our results for the spin-spin correlations are presented in Table II. As for the case $J<0$ we have not been able to perform a finite-size analysis but again we interpret the data in Table II as evidence for the existence of planar 120° Néel order in the GS of our model (17). This contradicts the prediction of the LSW analysis according to which one might have expected to find a ferromagnetic GS (see Sec. III E). However, one must recall that besides the 120° Néel GS and the ferromagnetic GS there are many more classical GS's. In a complete LSW analysis one would

TABLE II. Spin-spin correlations as in Table I, but for $J>0$. Sites j are numbered as in Fig. 9. For comparison the correlations $\langle S_0^x S_j^x + S_0^y S_j^y \rangle$ for the spin-1/2 Heisenberg AF on the triangular lattice are also displayed (data from [41]). Dots below a value for the correlation indicate that this value occurs repeatedly.

j	Classical	Triangular Heisenberg AFM	$N=21$		$N=24$
	$T=0$	$T=0$	$T=0$	$T=0.005J$	$T=0$
			1st neighbors		
1	−0.125	−0.125	−0.0847	−0.027	−0.0964
2	·	·	·	·	−0.0957
3	·	·	·	·	−0.0964
4	·	·	·	·	−0.0964
5	·	·	·	·	−0.0957
6	·	·	·	·	−0.0964
			2nd neighbors		
7	0.25	0.102	0.1352	0.050	0.163
8	·	·	·	·	0.1605
9	·	·	·	·	0.1605
10	·	·	·	·	0.1630
11	·	·	·	·	0.1605
12	·	·	·	·	0.1605
			3rd neighbors		
13	−0.125	−0.037	−0.0714	−0.022	−0.0830
14	·	·	·	·	−0.0833
15	·	·	·	·	−0.0830
16	·	·	·	·	−0.0830
17	·	·	·	·	−0.0833
18	·	·	·	·	−0.0830
			4th neighbors		
19	−0.125	−0.044	−0.0668	−0.019	−0.0799
20	·	·	·	·	−0.0799
21	·	·	·	·	−0.0799
22	·	·			−0.0799
			5th neighbor		
23	0.25	0.076			0.1563

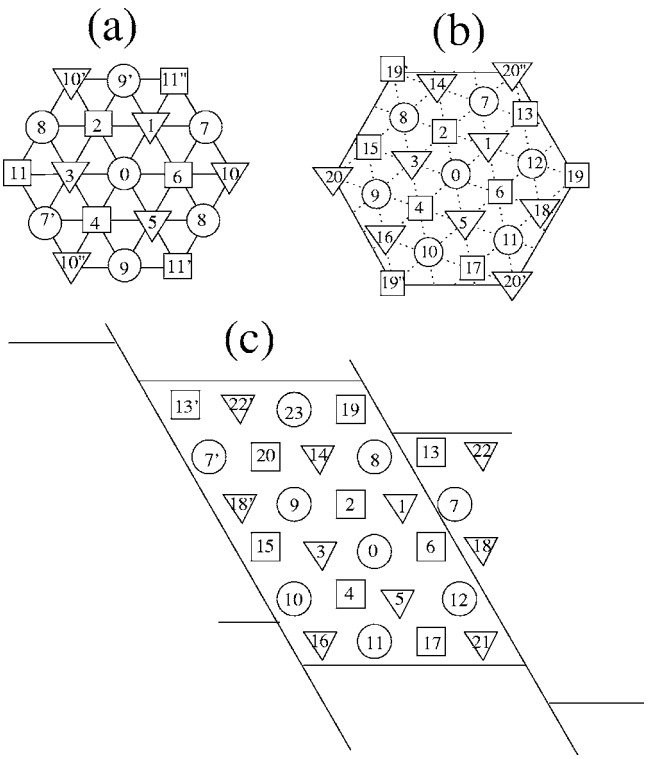

FIG. 9. (a) 12-, (b) 21-, and (c) 24-spin cell. ○, ▽, and ▽ mark the three sublattices. Primed sites belong to periodic repetitions of the cell containing the unprimed sites.

have to consider every one of these states, a task that is practically impossible to perform. Relative to the in-plane correlations the magnitude of out-of-plane correlations, which are not displayed in Table II, is even smaller here than in the case $J<0$. Further support for long-range order in the GS of the model (17) comes from a comparison of the spin-spin correlations of this model with the same correlations of the $=1/2$ Heisenberg AFM on the triangular lattice which we have included in Table II. It is seen there that the GS correlations of the model (17) decay more slowly than those of the GS of the TAF which is known to possess long-range 120° Néel order [33].

Additional strong support for existence of a Néel-ordered GS in both $J>0$ and $J<0$ cases comes from an investigation of chirality patterns. In both situations the quantum-mechanical calculation reveals that there exists a perfectly periodic pattern of chiralities χ_{ijk} as in the classical result. For $J>0$ we found that $\chi_{ijk}\approx\mp 0.5$ while for $J<0$ $\chi_{ijk}\approx\pm 0.69$. Both results are obtained in $N=21$, where the χ_{ijk} was calculated for six triangles located around the central site (Fig. 7). The $\mp,\pm$ notation indicates opposite chiralities between $J>0$ and $J<0$ results. A comparison of these values to ∓ 0.65 (Néel B configuration) and ± 0.65 (Néel A configuration) leaves little doubt on the nature of these GS's. Finally, please notice the excellent agreement between quantum and classical calculations for $J<0$.

Values for the spin-spin correlations of the model (17) for finite albeit small temperatures are also displayed in Table II. For $T=0.005J$ about 800 low-lying eigenstates were needed to achieve convergence in the data for the correlations. Although these finite-temperature correlations are smaller in magnitude than the GS correlations, they decay as slowly with the distance as the GS correlations, i.e., long-range order persists at finite temperatures. This is not surprising since our model (17) has *no continuous* symmetry. One thus expects the order to vanish at a finite temperature T_c in a first- or second-order phase transition. The temperature dependence of spin-spin correlations in the $N=21$ system is depicted in Fig. 10.

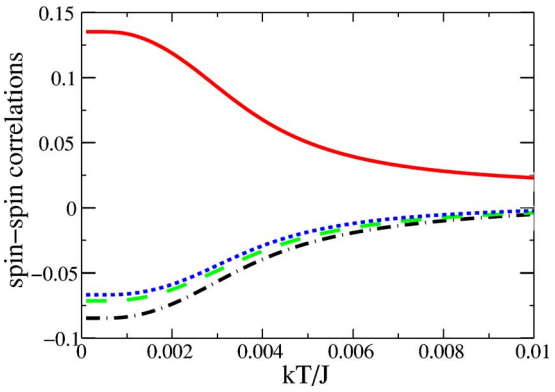

FIG. 10. (Color online) The curves from bottom to top correspond to in-plane spin-spin correlation to the first neighbor (black, dash-dotted), third neighbor (green, dashed), forth neighbor (blue, dotted), and second neighbor (red, solid). Two thousand lowest eigenstates were used in this calculation. The system size is $N=21$.

The finite-size effects affect the correlations very strongly for system sizes $N<21$. In Fig. 11 we plot the spin-spin correlations for the various system sizes. The data for $N=15,18$ are averages of the raw data for fixed lattice distances over the lattice directions. Because of boundary effects the correlations do not show the expected sixfold symmetry. As a consequence the data for $N=15,18$ cannot be used in a finite-size extrapolation. Nevertheless, despite these large finite size effects, for both cases $J>0$ and $J<0$ the GS energies can be reliably extracted from the data for all the cell sizes including the smaller ones. From the linear fits shown in Fig. 12 we obtain $E^A_{\rm GS}=-0.40|J|$ as the GS energy in case A. This is to be compared with the classical GS energy (see Sec. III D): $E^A_{\rm class}=-\frac{3}{2}\tau^2|J|=-0.375|J|(\tau=1/2)$. In the same way we find $E^B_{\rm GS}=-0.22J$ as the GS energy per site

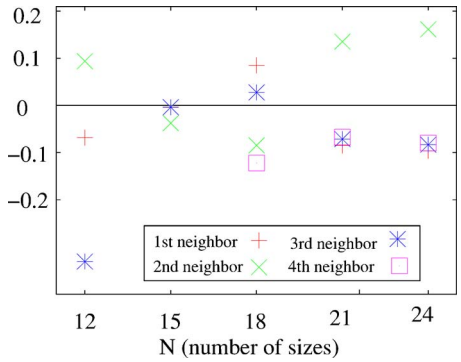

FIG. 11. (Color online) Spin-spin correlations for the various system sizes. The data for $N=15,18$ are averages of the raw data for fixed lattice distances over the lattice directions.

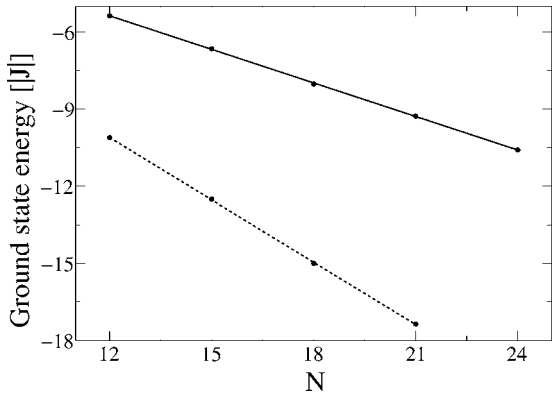

FIG. 12. Ground-state energies in units of $|J|$ as a function of the system size N. Solid (dashed) line is a linear fit to $J>0(J<0)$ data. The fit gives in the $J>0$ case $-0.22\,J\,N-0.07\,J$, while in the $J<0$ case $0.40\,J\,N+0.20\,J$.

in case B, which is to be compared to the classical GS energy (see Sec. III D) $E^B_{\text{class}}=-\frac{3}{4}\tau^2 J=-0.1875J$.

C. Low-energy spectra

Let us finally discuss the energy spectra of our model for both cases $J<0(A)$, and $J>0(B)$. Figures 13(a) and 13(b) show the accumulated density of states (accumulated DOS) of our model (17) for the two cases. On account of the breaking of the discrete symmetries of the Hamiltonian (17) by the 120° Neél order the standard expectation would be that the GS is sixfold degenerate for the *infinite* model and, since there is no continuous symmetry that could be broken, the excitations should be separated from the GS by a finite gap of the order of J. For *finite* systems the GS degeneracy will be lifted. Nevertheless, we expected to find six low-lying states in the gap below the lowest excited state. Figure 13(a), $J<0$, does not reflect this scenario convincingly. However, there are only a few states with energies substantially below $0.5|J|$. We take this as an indication of a gap of this order of magnitude in the spectrum of the Hamiltonian (17) in the thermodynamic limit $N\to\infty$.

Obviously, for $J>0$ the spectrum differs drastically from the above expectations; see Fig. 13(b). There is an abundance of very low-lying excitations, e.g., for $N=21$ there are about 2000 (800) states with energies less than $0.09J(0.05J)$ above the ground state. From the perfect symmetry of the finite-temperature spin-spin correlations and their relatively slow decay with temperature, we conclude that the majority of these excited eigenstates support the spin order of the GS.

Comparison of the lower panel of Fig. 13(b) with the scenario outlined above suggests that the gap, if any, is smaller than $0.5\times10^{-2}J$.

The rapid increase of the accumulated DOS that sets in at excitation energies of this order of magnitude leads to peaks in the specific heat,

$$\frac{1}{N}\frac{\partial}{\partial T}\frac{\sum_i E_i\exp[-E_i/(kT)]}{\sum_i \exp[-E_i/(kT)]}, \tag{23}$$

at the corresponding temperature. We have checked that the peak shifts toward lower temperatures as the size of the system increases. Indeed, in the $N=24$ system, we found the peak at $kT\approx2.5\times10^{-3}J$ while for $N=21$ it is at $kT\approx3.6\times10^{-3}J$; see Fig. 14 for the $N=21$ results. The precise determination of the peak position and amplitude in the $N=24$ system requires, however, a calculation based on more ex-

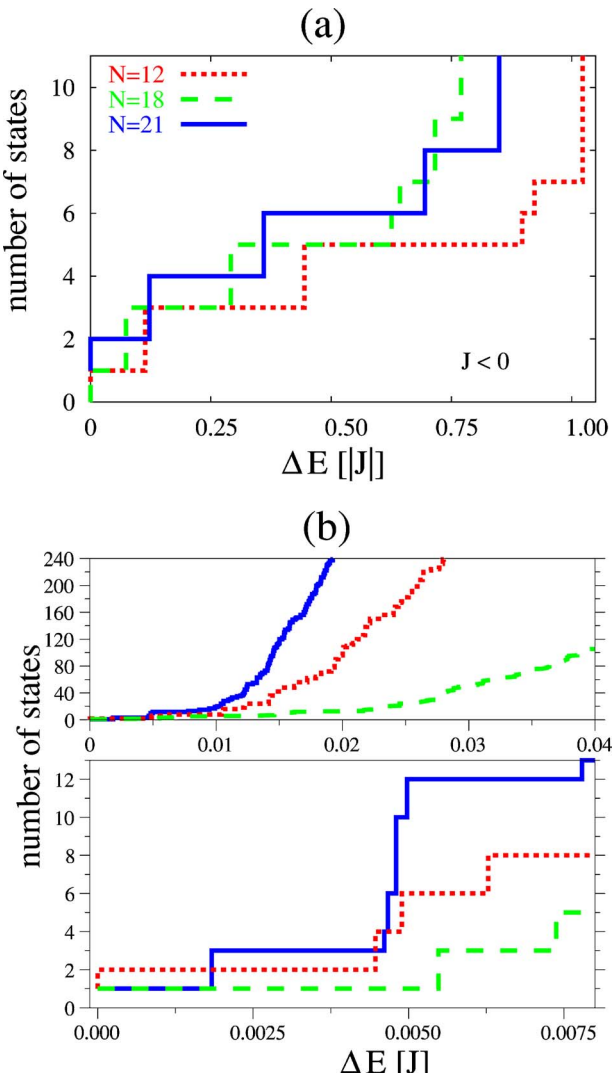

FIG. 13. (Color online) Accumulated density of states, i.e., the number of states in the energy interval ΔE above the ground state for (a) $J<0$ and (b) $J>0$. The curves in plot (b): blue (solid) $N=24$, red (dotted) $N=21$, and green (dashed) $N=18$.

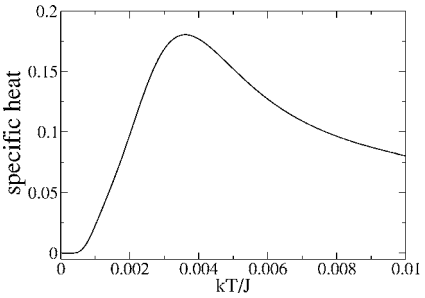

FIG. 14. Specific heat for $N=21$, Eq. (23). Two thousand lowest eigenstates were used in the formula (23) to prepare this plot.

cited eigenstates than we have been able to get [~ 240; see Fig. 13(b)]. The shift of the peak position between these two systems reflects the slightly different behavior of their accumulated DOS's. It would be very interesting to know whether this trend continues for larger N so that in the thermodynamic limit $N \to \infty$ the specific heat no longer decreases to zero at $T=0$. In this case our model (17) would be an example of a quantum model with a finite zero-temperature entropy.

Because of the strong finite-size effects in the data for $N<21$ the growth laws of the accumulated DOS with the system size N cannot be extracted reliably from our data. They are compatible, however, with an exponential increase of the number of low-lying states with N.

The features of the low-energy part of the spectrum of our model, Eq. (17), are strongly reminiscent of the low-energy part of the spin-1/2 Heisenberg antiferromagnet on the kagomé lattice [40,42]. There is, however, one decisive difference between the two models: while all GS correlations were found to be extremely short ranged [43] in the HAK there is, in all probability, long-range spin order in the GS of our model. The absence of long-range order in the HAK led Mila and Mambrini [38,39] to study the trimerized HAK in the basis consisting of all independent dimer coverings of the lattice by exclusively nearest-neighbor singlet pairs. By definition this restricted basis cannot produce any long-range order in the GS of the HAK. Using it in analytical and in numerical calculations Mila and Mambrini were able to reproduce the low-lying part of the spectrum of the HAK. In particular, they were able to determine the constant α in the growth law α^N that describes the increase of the number of low-lying states in the HAK. However, the approach of Mila and Mambrini is not suited for the treatment of our model for at least two reasons. (i) In contrast to the HAK our model is not SU(2) invariant. Therefore a restriction of the full Hilbert space of the model to exclusively singlet states is unwarranted. (ii) We need to describe spin-ordered states, and this is not possible in a basis consisting of products of nearest-neighbor singlet pairs. We suggest that for our model (17) the abundance of low-lying quantum states corresponds to the abundance of classical GS described in Sec. III D. Zero-point fluctuations lift the degeneracy of the classical states leaving the spin correlations that are built into these classical states qualitatively untouched. On account of its low-energy properties we have proposed the name quantum spin-liquid crystal for our system.

V. CONCLUSIONS

In this paper we have discussed in detail the physics of ultracold gases in trimerized kagomé lattices. Observation of this kind of physics, and detection of the predicted effects requires various steps: preparation of the trimerized lattice, loading of the considered gases, and detection. The first step, i.e., the preparation of the kagomé lattice, is discussed in detail in Sec. II A.

Probably the easiest experiment to perform concerns the observation of the unusual Mott phases of the Bose gas. Temperature requirements ($\simeq 100$ nK) are rather moderate. The challenging problem here is how to achieve 1/3, 2/3 fillings, etc. In principle physics should do it for us, since the "exotic" Mott phases are the thermodynamic phases of the system at zero temperature. There is, however, another elegant method of preparing such phases. To this aim one should start with a triangular lattice and achieve a Mott state with 1, 2, 3,… atoms per site. Then one should deform the lattice to a trimerized kagomé. The detection of such Mott phases can be done simply by releasing the atoms from the lattice, as in Ref. [3]. Coherence on the trimer level will then be visible in the appearance of interference fringes in time-of-flight images, which should reflect the on-trimer momentum distribution $\sim \Sigma_{i,j} \cos \vec{k}(\vec{r}_i - \vec{r}_j)$, where $\vec{r}_i$ are the positions of the minima in a trimer. In spite of the appearance of these fringes, the Mott-insulator nature of the state would be apparent in the presence of a gap for the excitations, which can be observed by tilting experiments as those of Ref. [3]. The opening of the gap should be analyzed as a function of the trimerization degree t'/t, which can be controlled as discussed in Sec. II A.

The experiment with a Fermi-Fermi mixture is more demanding. The main problem is, of course, the preparation of the states in the low-energy singlet sector. One possible way to prepare a singlet state in the trimerized kagomé lattice with $T<3t/4$ could employ the recently obtained Bose-Einstein condensates of molecules consisting of two fermionic atoms [62] at temperatures of the order of 10 nK. Such BEC's should be loaded onto an ideal and weak kagomé lattice. Note that the molecules formed after sweeping across a Feshbach resonance are in a singlet state of the pseudospin $\vec{s}$. This can easily be seen, because the two fermions enter the resonance from the s-wave scattering channel (i.e., in the symmetric state with respect to the spatial coordinates), and thus are in a singlet state of the pseudospin (i.e., antisymmetric state with respect to exchange of electronic and nuclear spins). Since the interaction leading to the spin flipping at the Feshbach resonance [63] is symmetric under the simultaneous interchange of both nuclear and electronic spins, then the formed molecule remains in a pseudospin singlet. The typical size of the molecule is of the order of the s-wave scattering length a, and thus can be modified at the resonance [64], being chosen comparable to the lattice wavelength. Growing the lattice breaks the molecule into two separate fermionic atoms in neighboring sites in the singlet pseudospin state. In this way, a singlet covering of the kagomé lattice may be achieved, allowing for the direct generation of a RVB state [65].

Assuming that we can prepare the system in a singlet state at $J'<T<J$, then the density of states of the low-lying singlet levels can be obtained by repeated measurements of the system energy. The latter can be achieved by simply releasing the lattice, so that after taking care of the zero-point energy, all of the interaction energy is transformed into kinetic energy. In a similar way we can measure the mean value and the distribution of any nearest-neighbor two-spin correlation functions. With this aim one has to apply at the moment of the trap release a chosen nearest-neighbor two-spin Hamiltonian and keep it acting during the cloud expansion (for details see [25]). In a similar manner we can measure the spectrum of triplet excitation, by exciting a triplet

state, which can be done by flipping one spin using a combination of superlattice methods and laser excitation [66]. The measurement of the singlet-triplet gap requires a resolution better than J'.

A similar type of measurements can be performed in the ideal kagomé lattice, when $J=J'$. In this case, the singlet-triplet gap is filled with singlet excitations [42]. By varying ϕ, one can transform adiabatically from strongly trimerized to ideal Kagomé, for which the final value of J will be smaller than the initial J, but larger than the initial J'. In that case, the system should remain within the lowest set of 1.15^N states that originally formed the lowest singlet band. The singlet-triplet gap, if any, is estimated to be $\leqslant J/20$, and should be measurable using the methods described above.

The observation of properties of the spinless interacting Fermi gas is also experimentally very challenging. The first step is to create the interacting Fermi gas, obviously. As we discussed in Sec. III A this can be achieved with either dipolar particles, or composite fermions. Both of these possibilities are challenging themselves, although the rapid progress in cooling and trapping of dipolar atoms [55] and molecules allows one to hope that interacting spinless Fermi gases will be routinely available in the next future. Preparing of the 2/3 filling is also a challenge, but several routes have been proposed in Sec. III A. Yet another challenge is to measure the predicted properties of the quantum spin-liquid crystal.

One quantity which should be possible to measure relatively easy, is the energy of the system. This can be done simply by opening the lattice; by repeated measurement of the energy $E(T)$ at (definite) finite temperatures one would get in this way an access to the density of modes, i.e., one could compare the results with Fig. 13. From such measurements one could infer the existence of a gap E_{gap}, since, if E_{gap} is large enough, $E(T)$ becomes T independent for $kT \leqslant E_{\mathrm{gap}}$. Various other correlations could be measured using the methods proposed in Ref. [25]. In order to measure planar spin correlations, one has, however, to lift the degeneracy of the $f_{\pm}$ modes, e.g., by slightly modifying the intensity of one of the superlattices forming the trimerized lattice. This should be done on a time scale faster than the characteristic time scales of other interactions, so that the state of the system would not change during the measurement. In such a case one can use far-off-resonant Raman scattering (or scattering of matter waves) to measure the dynamic structure factor, which is proportional to the spatiotemporal Fourier transform of the density-density correlations. At frequencies close to the two photon Raman resonance between the $f_{\pm}$ modes, only f_+-f_- transitions contribute to the signal, and hence such measurement yields the desired information about the correlations $\langle f_+^{(i)\dagger} f_-^{(i)} f_-^{(j)\dagger} f_+^{(j)} \rangle$, and the spin correlations of Figs. 10 and 11 and Tables I and II.

ACKNOWLEDGMENTS

We acknowledge discussions with M. Greiner, R. Grimm, and P. Julienne. We are especially indebted to A. Honecker for his collaboration on this project. This paper has been supported by the Deutsche Forschungsgemeinschaft (SFB 407, Grants No SPP1116, No. 436POL), the ESF program QUDEDIS, the Russian Foundation for Basic Research, the Alexander von Humboldt Foundation, and the U.S. Department of Energy.

APPENDIX A: CALCULATION OF THE PARAMETERS FOR THE HUBBARD HAMILTONIAN

1. Wannier functions

For periodic boundary conditions the linear part of the Hamiltonian (5) can be diagonalized in the quasimomentum space using the scheme of Bloch [47]. In the kagomé lattice a single cell contains three equivalent potential minima, and hence three Wannier functions per unitary cell are required, which can be obtained by transforming the Bloch states of the first three bands into the Wannier basis. Let us first consider one particle that is placed in an isolated trimer. The Hamiltonian for this model reads $H=-t\{c_1^\dagger c_2+c_2^\dagger c_3+c_3^\dagger c_1 +\mathrm{H.c.}\}$. The eigenfunctions of H are $\vec{a}_0=(1,1,1)^T/\sqrt{3}, \vec{a}_1 =(-2,1,1)^T/2$, and $\vec{a}_2=(0,-1,1)^T/\sqrt{2}$ with respective eigenvalues $\{-2t,t,t\}$. The transformation matrix $(\vec{a}_0,\vec{a}_1,\vec{a}_2)^{-1}$ leads to the states for which just one site of the triangle is occupied. A similar scheme can also be applied for the Bloch functions $\psi_k^i(\mathbf{r})=e^{-i\mathbf{k}\cdot\mathbf{r}}u_{\mathbf{k}}^i(\mathbf{r})$, where $\mathbf{k}$ is the quasimomentum, and $u_{\mathbf{k}}^i(\mathbf{r})$ are the periodic functions of band i. For a particular quasimomentum $\mathbf{k}$, the values of $u_{\mathbf{k}}^i(\mathbf{r})$ at the potential minima are $a_{ij}(\mathbf{k})$, where $j\in\{1,2,3\}$ denotes the minimum within the trimer (Fig. 6). Inverting the matrix a_{ij} for a particular $\mathbf{k}$ one obtains complex coefficients c_{op}, which are then used to construct a periodic function having its maximum in only one of the three potential minima: $w_{\mathbf{k}}^o =\Sigma_i c_{oi}u_{\mathbf{k}}^i$, where $o=\{1,2,3\}$ denotes the corners of the trimer. Similarly as the $u_{\mathbf{k}}^i$, the $w_{\mathbf{k}}^o$ are functions with the same periodicity as the lattice. Summation of these functions over $\mathbf{k}$ with a proper phase leads to the Wannier functions [67]: $W_{\mathbf{R}}^o=(1/N_l)\Sigma_{\mathbf{k}}e^{i\mathbf{k}\cdot\mathbf{R}}w_{\mathbf{k}}^o$, where $\mathbf{R}$ denotes the position of the particular trimer on which the maximum of the Wannier functions is located.

The point-group symmetry of the lattice is broken due to the choice of the particular set of basis vectors for the reciprocal lattice. A direct consequence of this fact is that the Wannier functions within a trimer cannot be transformed into each other by a rotation of $\pm 2/3\pi$ around the center of the trimer. Hence one obtains different hopping probabilities between the sites of the triangle, $t_{ij}=\langle W_{\mathbf{R}}^i|H_0|W_{\mathbf{R}}^j\rangle =(1/N_l^2)\Sigma_{\mathbf{k}}\Sigma_{\mu}c_{i,\mu}c_{j,\mu}\epsilon_{\mathbf{k}}^{\mu}$ where $\epsilon_{\mathbf{k}}^{\mu}$ is the energy for the quasimomentum $\mathbf{k}$ in band μ. The Wannier functions can be symmetrized by summing up Bloch functions multiplied with a $\mathbf{k}$-dependent phase factor $e^{-i\mathbf{k}\cdot\mathbf{r}_i}$, where $\mathbf{r}_i$ is the position of one of the three potential minima within a cell. The hopping elements change then to $t_{ij}=(1/N_l^2)\Sigma_{\mathbf{k}}\cos\mathbf{k}\cdot(\mathbf{r}_i -\mathbf{r}_j)\Sigma_o c_{i,o}c_{j,o}\epsilon_{\mathbf{k}}^o$, which are independent of the position now. The cost of the symmetrization is that the Wannier functions are not orthogonal anymore, but the overlap remains relatively small.

2. Gaussian ansatz

Apart from the case of the kagomé lattice, it is difficult to obtain the Wannier functions reliably. The coefficients for the Hubbard-Hamiltonian can be alternatively obtained using a Gaussian ansatz [68], which, in the case of a perfect kagomé lattice, and for deep lattice potentials above $5E_{\mathrm{rec}}$ leads to results which are practically indistinguishable from those of the Wannier functions. The shape of the Gaussian function reads $f(x,y)=\sqrt{2/(\sigma_x\sigma_y\pi)}\exp(-x^2/\sigma_x^2)\exp[-(y-y_0)^2/\sigma_y^2]$. The center y_0, and the widths σ_x and σ_y are the variational parameters minimizing the energy functional: $E=\int_{-\infty}^{\infty}dx\int_{-\infty}^{\infty}dy[\nabla(f(x,y))^2+f(x,y)^2V(x,y)]$. The Gauss functions for the other two minima in the trimer are obtained by rotating the Gaussian function by $\pm\frac{2}{3}\pi$ around the center of the trimer.

APPENDIX B: MEAN-FIELD THEORY FOR A BOSONIC GAS

The boundaries between Mott insulator and superfluid phases can be obtained by means of a mean-field approach similar to that employed in Ref. [21]. We consider only on-site contact-interaction terms, but contrary to Ref. [21] we do not restrict ourselves to the hard-core limit. The system is governed by a Bose-Hubbard Hamiltonian of the form $H=H_{\mathrm{tr}}+H_{\mathrm{hop}}$, with

$$H_{\mathrm{tr}}=-t\sum_{\langle ij\rangle}(b_i^\dagger b_j+\mathrm{H.c.})+\frac{1}{2}\sum_i n_i(n_i-1)-\mu\sum_i n_i, \tag{B1}$$

$$H_{\mathrm{hop}}=-t'\sum_{\langle kl\rangle}(b_k^\dagger b_l+\mathrm{H.c.}), \tag{B2}$$

where t,t' (denoting the intra- and intertrimer hoppings) and μ are measured in units of the on-site interaction potential U.

Assuming a fixed number of atoms n per trimer, we consider all possible Fock states of the form $|n_1n_2n_3\rangle$ with $n_1+n_2+n_3=n$. For example, for one particle per trimer the Hilbert space contains the Fock states $|100\rangle,|010\rangle$, and $|001\rangle$. Since the model is invariant under rotation of $2\pi/3$ the eigenstates are of the form $|W_1\rangle=(|100\rangle+z|010\rangle+z^2|001\rangle)/\sqrt{3}$, with $z\in\{1,\exp(i\frac{2}{3}\pi),\exp(-i\frac{2}{3}\pi)\}$, implying states with no, left, and right chirality, also known as W states [49]. We denote $z_\pm=\exp(\pm i2\pi/3)$ and introduce the operators $B_\pm=(b_1+z_\pm b_2+z_\pm^2 b_3)/\sqrt{3}, B_0=(b_1+b_2+b_3)/\sqrt{3}$. Their commutation relations are $[B_\alpha,B_\beta^\dagger]=\delta_{\alpha\beta},\alpha,\beta=\{0,+,-\}$. The chirality operator is defined as $\chi=(B_+^\dagger B_+-B_-^\dagger B_-)$ mod 3. Equation (B1) can be rewritten into the form

$$\begin{aligned}H_{\mathrm{tr}}=&-t3B_0^\dagger B_0+(t-\mu)\{B_0^\dagger B_0+B_+^\dagger B_++B_-^\dagger B_-\}+\tfrac{1}{6}\{(B_0^{\dagger 2}\\&+2B_+^\dagger B_-^\dagger)(B_0^2+2B_+B_-)+(B_+^{\dagger 2}+2B_0^\dagger B_-^\dagger)(B_+^2+2B_0B_-)\\&+(B_-^{\dagger 2}+2B_0^\dagger B_+^\dagger)(B_-^2+2B_0B_+)\}.\end{aligned} \tag{B3}$$

Therefore $[\exp i2\pi/3(B_+^\dagger B_+-B_-^\dagger B_-),H_{\mathrm{tr}}]=0$, and hence the chirality of a state is a conserved quantity. It can be shown that the ground state has chirality zero, and therefore we restrict ourselves henceforth to these states.

For a given number of particles n per trimer, we denote by $|W_n^\mu\rangle$ a particular normalized nonchiral sum of permutations of a set n_1,n_2,n_3, where μ denotes different allowed nonchiral states. For example, for two particles per trimer, two possible states are allowed: $|W_2^1\rangle=(|110\rangle+|101\rangle+|011\rangle)/\sqrt{3}$ and $|W_2^2\rangle=(|200\rangle+|020\rangle+|002\rangle)/\sqrt{3}$. We can then diagonalize the Hamiltonian H_{tr} in this basis, $H_n^{\alpha\beta}=\langle W_n^\alpha|H_{\mathrm{tr}}|W_n^\beta\rangle$, obtaining the eigenenergies ϵ_n^l and eigenstates $|\psi_n^l\rangle$, where $0\leqslant l\leqslant n$. The lowest energies ϵ_n^0 for each particle number n have to be compared to obtain the ground state in the $(t-\mu)$-phase space.

If the intertrimer hopping t' is small, the phase boundaries in the $t-t'-\mu$ phase diagram can be well estimated by using a mean-field approach [19,51,52]. We introduce the superfluid order parameter $\psi=\langle b_i\rangle=\langle b_i^\dagger\rangle$, for every site i. Neglecting fluctuations of $b_i,b_j^\dagger$ in the second order, we can substitute $b_j^\dagger b_i=\psi(b_j^\dagger+b_i)-\psi^2$, and hence H_{hop} can be decomposed into a sum of single-site Hamiltonians of the form $H_{\mathrm{hop}}\approx 6t'\psi^2-2\sqrt{3}t'\psi(B+B^\dagger)$. The Hamiltonian H can be decomposed then into two parts $H=H_0+V$, with $H_0=H_{\mathrm{tr}}+6t'\psi^2$ and $V=-2t'\sqrt{3}\psi(B_0+B_0^\dagger)$, where H_0 is perturbed by V. Up to second-order perturbation theory, the energy becomes of the form $E=\epsilon_n^0+r\psi^2$, where

$$r=6t'\psi^2+\sum_{m=n\pm1,i}\frac{|\langle\psi_n^0V\psi_m^i\rangle|^2}{\epsilon_n^0-\epsilon_m^i}. \tag{B4}$$

The Mott insulator to superfluid transition may be identified by the equation $r=0$, since for $r>0$ the energy is minimized for ψ^2 is zero, and for $r<0$ ψ acquires a finite value. The equation $r=0$ defines a 2D manifold in the $t'-t-\mu$ parameter space.

As an example, we determine in this appendix the expression for the boundaries of the Mott phase with one particle per trimer. Due to the form of Eq. (B4) this calculation demands the knowledge of the eigenenergies and eigenfunctions for $n=1$ and 2. For $n=1$, $|\psi_1^0\rangle=(|001\rangle+|010\rangle+|100\rangle)/\sqrt{3}=B^\dagger|\psi_0\rangle$ and $\epsilon_1^0=\langle\psi_1^0|H_{\mathrm{tr}}|\psi_1^0\rangle=-\mu-2t$. For $n=2$,

$$\epsilon_2^{0,1}=\frac{1}{2}(1\mp\sqrt{(1+2t)^2+32t^2})-t-2\mu, \tag{B5}$$

and $|\psi_2^{0,1}\rangle=\cos\phi_{0,1}|W_2^2\rangle+\sin\phi_{0,1}|W_2^1\rangle$, with

$$\tan\phi_{0,1}=\frac{1}{4\sqrt{2t}}\{(1+2t)\mp\sqrt{(1+2t)^2+32t^2}\}. \tag{B6}$$

At $t'=0$ the region of one particle per trimer is provided by the condition $0\leqslant\epsilon_1^0\leqslant\epsilon_2^0$, i.e., when $-2t\leqslant\mu\leqslant t+[1-\sqrt{(1+2t)^2+32t^2}]/2$.

After a straightforward but tedious calculation, we can then calculate the sum in Eq. (B4),

$$\sum_{m=0,2,i} \frac{|\langle \psi_1^0 | V | \psi_m^i \rangle|^2}{\epsilon_1^0 - \epsilon_m^i} = 4t'^2 \psi^2 \left(\frac{(6\mu - 24t - 4)}{\mu^2 - \mu(2t+1) - 8t^2} - \frac{3}{2t+\mu} \right). \tag{B7}$$

Hence, solving for $r=0$, we obtain the value of t' at the phase boundary:

$$t' = \frac{1/2(\mu^2 - \mu(2t+1) - 8t^2)(2t+\mu)}{(\mu+8t)(2t+1/3) - \mu^2 - 8t^2}. \tag{B8}$$

[1] M. H. Anderson, J. R. Ensher, M. R. Matthews, C. E. Wieman, and E. A. Cornell, Science **269**, 198 (1995); K. B. Davis, M.-O. Mewes, M. R. Andrews, N. J. van Druten, D. S. Durfee, D. M. Kurn, and W. Ketterle Phys. Rev. Lett. **75**, 3969 (1995); C. C. Bradley, C. A. Sackett, J. J. Tollett, and R. G. Hulet, *ibid.* **75**, 1687 (1995).

[2] D. Jaksch, C. Bruder, J. I. Cirac, C. W. Gardiner, and P. Zoller, Phys. Rev. Lett. **81**, 3108 (1998).

[3] M. Greiner, O. Mandel, T. Esslinger, T. W. Hansch, and I. Bloch, Nature (London) **415**, 39 (2002); M. Greiner, O. Mandel, T. W. Hansch, and I. Bloch, *ibid.* **419**, 51 (2002).

[4] BCS denotes the Bardeen-Schrieffer-Cooper transition to a SF state in a Fermi gas or liquid; for the recent results on the BCS-BEC crossover see C. Chin, M. Bartenstein, A. Altmeyer, S. Riedl, S. Jochim, J. H. Denschlag, and R. Grimm, Science **305**, 1128 (2004); for theory see J. Kinnunen, M. Rodriguez, and P. Torma, *ibid.* **305**, 1131 (2004); see also M. W. Zwierlein, C. A. Stan, C. H. Schunck, S. M. F. Raupach, A. J. Kerman, and W. Ketterle, Phys. Rev. Lett. **92**, 120403 (2004); M. W. Zwierlein, C. H. Schunck, C. A. Stan, S. M. F. Raupach, and W. Ketterle, *ibid.* **94**, 180401 (2005); M. Greiner, C. A. Regal, and D. S. Jin, *ibid.* **94**, 070403 (2005); J. Zhang, E. G. M. Van Kempen, T. Bourdel, L. Khaykovich, J. Cubizolles, F. Chevy, M. Teichmann, L. Tarruell, S. J. J. M. F. Kokkelmans, and C. Salomon, e-print cond-mat/0410167; M. Bartenstein, A. Altmeyer, S. Riedl, S. Jochim, R. Geursen, C. Chin, J. H. Denschlag, and R. Grimm, e-print cond-mat/0412712.

[5] N. K. Wilkin and J. M. F. Gunn, Phys. Rev. Lett. **84**, 6 (2000); B. Paredes, P. Fedichev, J. I. Cirac and P. Zoller, *ibid.* **87**, 010402 (2001).

[6] B. Paredes, A. Widera, V. Murg, O. Mandel, S. Folling, I. Cirac, G. V. Shlyapnikov, T. W. Hansch, and I. Bloch, Nature (London) **429**, 277 (2004).

[7] A. Osterloh, L. Amico, G. Falci, and R. Fazio, Nature (London) **416**, 608 (2002); T. J. Osborne and M. A. Nielsen, Phys. Rev. A **66**, 032110 (2002); W. K. Wootters, Contemp. Math. **305**, 299 (2002); K. M. O'Connor and W. K. Wootters, Phys. Rev. A **63**, 052302 (2001); G. Vidal, J. I. Latorre, E. Rico, and A. Kitaev, Phys. Rev. Lett. **90**, 227902 (2003); J. I. Latorre, E. Rico, and G. Vidal, Quantum Inf. Comput. **4**, 48 (2004); T. Meyer, U. V. Poulsen, K. Eckert, M. Lewenstein, and D. Bruβ, Int. J. Quantum Inf. **2**, 149 (2004); A. Hutton and S. Bose, Phys. Rev. A **69**, 042312 (2004); F. Verstraete, M. Popp and J. I. Cirac, Phys. Rev. Lett. **92**, 027901 (2004); F. Verstraete, M. A. Martin-Delgado, and J. I. Cirac, Phys. Rev. Lett. **92**, 087201 (2004).

[8] G. Vidal, Phys. Rev. Lett. **93**, 040502 (2004); F. Verstraete, D. Porras, and J. I. Cirac, *ibid.* **93**, 227205 (2004); S. R. Clark and D. Jaksch, Phys. Rev. A **70**, 043612 (2004); A. J. Daley, C. Kollath, U. Schollwöck, and G. Vidal, J. Stat. Mech.: Theory Exp. 2004, P04005.

[9] R. Grimm, M. Weidemüller, and Y. B. Ovchinnikov, Adv. At., Mol., Opt. Phys. **42**, 95 (2000).

[10] L.-M. Duan, E. Demler, and M. D. Lukin, Phys. Rev. Lett. **91**, 090402 (2003).

[11] L. Santos, M. A. Baranov, J. I. Cirac, H.-U. Everts, H. Fehrmann, and M. Lewenstein, Phys. Rev. Lett. **93**, 030601 (2004).

[12] G. Grynberg, B. Lounis, P. Verkerk, J.-Y. Courtois, and C. Salomon, Phys. Rev. Lett. **70**, 2249 (1993); K. I. Petsas, A. B. Coates, and G. Grynberg, Phys. Rev. A **50**, 5173 (1994); L. Guidoni and P. Verkerk, *ibid.* **57**, R1501 (1998); P. Rabl, A. J. Daley, P. O. Fedichev, J. I. Cirac, and P. Zoller, Phys. Rev. Lett. **91**, 110403 (2003).

[13] D. Jaksch, H.-J. Briegel, J. I. Cirac, C. W. Gardiner, and P. Zoller, Phys. Rev. Lett. **82**, 1975 (1999).

[14] O. Mandel, M. Greiner, A. Widera, T. Rom, T. W. Hansch, and I. Bloch, Nature (London) **425**, 6961 (2003).

[15] J. I. Cirac and P. Zoller, Phys. Today **57**(3), 38 (2004); for the original idea of quantum simulators see R. P. Feynman, Found. Phys. **16**, 507 (1986).

[16] A. Auerbach, *Interacting Electrons and Quantum Magnetism* (Springer, New York, 1994).

[17] F. H. L. Essler, H. Frahm, F. Göhmann, A. Klümper and V. E. Korepin, *The One-Dimensional Hubbard Model* (Cambridge University Press, Cambridge, U.K., 2005).

[18] D. Jaksch and P. Zoller, Ann. Phys. (N.Y.) **315**, 52 (2005).

[19] M. P. A. Fisher, P. B. Weichman, G. Grinstein, and D. S. Fisher, Phys. Rev. B **40**, 546 (1989).

[20] W. Hofstetter, J. I. Cirac, P. Zoller, E. Demler, and M. D. Lukin, Phys. Rev. Lett. **89**, 220407 (2002).

[21] M. Lewenstein, L. Santos, M. A. Baranov, and H. Fehrmann, Phys. Rev. Lett. **92**, 050401 (2004).

[22] A. P. Albus, F. Illuminati, and M. Wilkens, Phys. Rev. A **67**, 063606 (2003); H. P. Büchler and G. Blatter, Phys. Rev. Lett. **91**, 130404 (2003); A. B. Kuklov and B. V. Svistunov, *ibid.* **90**, 100401 (2003); H. Fehrmann, M. A. Baranov, B. Damski, M. Lewenstein, and L. Santos, Opt. Commun. **243**, 23 (2004).

[23] B. Damski, J. Zakrzewski, L. Santos, P. Zoller, and M. Lewenstein, Phys. Rev. Lett. **91**, 080403 (2003).

[24] A. Sanpera, A. Kantian, L. Sanchez-Palencia, J. Zakrzewski, and M. Lewenstein, Phys. Rev. Lett. **93**, 040401 (2004).

[25] J. J. García-Ripoll and J. I. Cirac, Philos. Trans. R. Soc. London, Ser. A **361**, 1537 (2003); J. J. García-Ripoll, M. A. Martin-Delgado, and J. I. Cirac, Phys. Rev. Lett. **93**, 250405 (2004).
[26] U. Dorner, P. Fedichev, D. Jaksch, M. Lewenstein, and P. Zoller, Phys. Rev. Lett. **91**, 073601 (2003).
[27] F. Mintert and C. Wunderlich, Phys. Rev. Lett. **87**, 257904 (2001); D. Porras and J. I. Cirac, *ibid.* **92**, 207901 (2004); D. Porras and J. I. Cirac, Laser Phys. **15**, 88 (2005).
[28] W. Dür, L. Hartmann, M. Hein, M. Lewenstein, and H.-J. Briegel, Phys. Rev. Lett. **94**, 097203 (2005).
[29] G. Misguich and C. Lhuillier, in *Frustrated Spin Systems*, edited by H. T. Diep (World Scientific, Singapore, 2005); C. Lhuillier, e-print cond-mat/0502464.
[30] C. Lhuillier, P. Sindzingre, and J.-B. Fouet, Can. J. Phys. **79**, 1525 (2001).
[31] B. Sutherland, *Beautiful Models, 70 Years of Exactly Solved Quantum Many-Body Problems* (World Scientific, Singapore, 2004).
[32] S. Rapsch, U. Schollwöck, and W. Zwerger, Europhys. Lett. **46**, 559 (1999).
[33] B. Bernu, C. Lhuillier, and L. Pierre, Phys. Rev. Lett. **69**, 2590 (1992). B. Bernu, P. Lecheminant, C. Lhuillier, and L. Pierre, Phys. Rev. B **50**, 10048 (1994).
[34] I. Affleck, T. Kennedy, E. H. Lieb, and H. Tasaki, Commun. Math. Phys. **115**, 477 (1988).
[35] O. A. Starykh, A. Furusaki, and L. Balents, Phys. Rev. B **72**, 094416 (2005).
[36] S. Dommange, M. Mambrini, B. Normand, and F. Mila, Phys. Rev. B **68**, 224416 (2003).
[37] V. Subrahmanyam, Phys. Rev. B **52**, 1133 (1995).
[38] F. Mila, Phys. Rev. Lett. **81**, 2356 (1998).
[39] M. Mambrini and F. Mila, Eur. Phys. J. B **17**, 651 (2000).
[40] P. Lecheminant, B. Bernu, C. Lhuillier, L. Pierre, and P. Sindzingre, Phys. Rev. B **56**, 2521 (1997).
[41] P. Lecheminant, Thèse de Doctorat de l'Université Paris 6, 1995 (unpublished).
[42] C. Waldtmann, H.-U. Everts, B. Bernu, C. Lhuillier, P. Sindzingre, P. Lecheminant, and L. Pierre, Eur. Phys. J. B **2**, 501 (1998).
[43] P. W. Leung and V. Elser, Phys. Rev. B **47**, 5459 (1993).
[44] K. Hida, J. Phys. Soc. Jpn. **69**, 4003 (2000).
[45] P. Nikolic and T. Senthil, Phys. Rev. B **68**, 214415 (2003).
[46] B. Damski, H.-U. Everts, A. Honecker, H. Fehrmann, L. Santos, and M. Lewenstein, Phys. Rev. Lett. **95**, 060403 (2005).
[47] N. W. Ashcroft and D. N. Mermin, *Solid State Physics* (Holt, Rinehart and Winston, Phyiladelphia, 1976).
[48] For dipolar lattice gases, see K. Góral, L. Santos, and M. Lewenstein, Phys. Rev. Lett. **88**, 170406 (2002); for a general review, see M. A. Baranov, L. Dobrek, K. Góral, L. Santos, and M. Lewenstein, Phys. Scr., T **102**, 74 (2002).
[49] W. Dür, G. Vidal, and J. I. Cirac, Phys. Rev. A **62**, 062314 (2000).
[50] J. Joo, Y. J. Park, S. Oh, and J. Kim, New J. Phys. **5**, 136 (2003).
[51] S. Sachdev, *Quantum Phase Transitions* (Cambridge University Press, Cambridge, U.K., 1999).
[52] D. van Oosten, P. van der Straten, and H. T. C. Stoof, Phys. Rev. A **63**, 053601 (2001).
[53] P. Buonsante, V. Penna, and A. Vezzani, Phys. Rev. A **70**, 061603(R) (2004); Laser Phys. **15**, 361 (2005).
[54] P. Buonsante and A. Vezzani, Phys. Rev. A **72**, 013614 (2005).
[55] A. Griesmaier, J. Werner, S. Hensler, J. Stuhler, and T. Pfau, Phys. Rev. Lett. **94**, 160401 (2005).
[56] B. Damski, L. Santos, E. Tiemann, M. Lewenstein, S. Kotochigova, P. Julienne, and P. Zoller, Phys. Rev. Lett. **90**, 110401 (2003).
[57] A. J. Daley, P. O. Fedichev, and P. Zoller, Phys. Rev. A **69**, 022306 (2004).
[58] S. Miyashita, Prog. Theor. Phys. Suppl. **87**, 112 (1986).
[59] T. Jolicoeur and J. C. Le Guillou, Phys. Rev. B **40**, 2727 (1989).
[60] A. B. Harris, C. Kallin, and A. J. Berlinsky, Phys. Rev. B **45**, 2899 (1992).
[61] http://www.caam.rice.edu/software/ARPACK/
[62] S. Jochim, M. Bartenstein, A. Altmeyer, G. Hendl, S. Riedl, C. Chin, J. H. Denschlag, and R. Grimm, Science **302**, 2101 (2003); M. Greiner, C. A. Regal, and D. S. Jin, Nature (London) **426**, 537 (2003); M. W. Zwierlein, C. A. Stan, C. H. Schunck, S. M. F. Raupach, S. Gupta, Z. Hadzibabic, and W. Ketterle, Phys. Rev. Lett. **91**, 250401 (2003).
[63] E. Timmermans, P. Tommasini, M. Hussein, and A. Kerman, Phys. Rep. **315**, 199 (1999).
[64] D. S. Petrov, C. Salomon, and G. V. Shlyapnikov, Phys. Rev. Lett. **93**, 090404 (2004).
[65] P. W. Anderson, Mater. Res. Bull. **8**, 153 (1973).
[66] I. Bloch (private communication).
[67] W. Kohn, Phys. Rev. **115**, 809 (1959).
[68] P. Pedri, L. Pitaevskii, S. Stringari, C. Fort, S. Burger, F. S. Cataliolti, P. Maddalsni, F. Minardi, and M. Inguscio, Phys. Rev. Lett. **87**, 220401 (2001).